Aerospace Science and Technology 106 (2020) 106083

Contents lists available at ScienceDirect

Aerospace Science and Technology

www.elsevier.com/locate/aescte

Dynamic analysis of folded laminated composite plate using nonpolynomial shear deformation theory

Babu Ranjan Thakur *, Surendra Verma, B.N. Singh, D.K. Maiti

Department of Aerospace Engineering, Indian Institute of Technology Kharagpur, W. Bengal 721302, India

ARTICLE INFO

Article history:
Received 25 March 2020
Received in revised form 23 June 2020
Accepted 14 July 2020
Available online 12 August 2020
Communicated by Pinqi Xia

Keywords:
Folded plate
Composite plate
Finite element method
Free vibration
Forced vibration
Nonpolynomial shear deformation theory (NPSDT)

ABSTRACT

In this paper, an efficient C^0 finite element modeling based on higher-order nonpolynomial shear deformation theory (NPSDT) is proposed for the dynamic analysis of folded laminated composite plate. The theoretical formulations are based on nine-noded Lagrange isoparametric finite element and inverse hyperbolic shear deformation theory (IHSDT) as NPSDT. The employed theory, IHSDT, assumes the nonlinear and realistic distribution of transverse shear stresses, and also satisfies the traction-free boundary conditions at the top and bottom surfaces of the plate. Hamilton's principle has been adopted to derive the system's governing equation. A penalty approach has been used to take into account the artificial constraints generated due to incorporation of C^0 Lagrange element. The free vibration pertaining to eigenvalue problem is solved using subspace iteration method. The transient analysis subjected to pressure load and vertical load is carried out using Newmark's direct integration scheme. The formulation has been validated with the available solution in the literature, and several novel solutions have been proposed to address the various practical aspects of folded plate. Numerical illustrations are presented to investigate the effect of various parameters such as crank angle, fiber angle, lamination scheme, fold location, and boundary conditions on the natural frequency and transient response of laminated composite plate.

1. Introduction

The advent of fiber-reinforced laminated composites brought a revolution in the field of structural design and manufacturing due to their high specific stiffness, high strength, and other mechanical properties such as, better tailoring ability through the varying lamination sequence and fiber orientation to meet the specific demand of the application. These advancements in the material properties resulted into the multifaceted utilization of laminated composite plate in various industries. That is why, it encompasses almost all the realm of structural design and manufacturing. Furthermore, structural engineering requires various kinds of structures to be analyzed for the better design and implementation; one such type is the folded plate structure. This type of structure is widely employed in the aircraft fuselages, winglet, vehicle chassis, ship hulls, buildings and bridges, etc. Moreover, the fold geometry structures are verily found in nature as well, such as palm leaves, seashells, etc. So, to understand the folded structure and its dynamic behavior, an extensive analysis need to be carried out considering all the facets of composite.

Initial work in this regard is pioneered by Goldberg and Leve [1] who investigated the exact static analysis of folded plate structures. Latter, Irie et al. [2] utilized Ritz method to calculate the natural frequencies of cantilever folded plates with and without structural symmetry. Ohga and Shinematsu [3] investigated the bending problem of folded plates employing boundary element-transfer matrix method as this method allows them to use for the large number of elements without dealing with the large matrices. Latter, several researchers employed various methods to model the mechanical behavior of folded structures, like finite strip method [4–6], transfer matrix method [7,8], spectral element method [9,10], etc. Further, Duan and Miyamoto [11] developed an effective hybrid/mixed shell element for the analysis of folded plate and curved shell by assuming compatible, non-compatible displacement and stress fields. Hernandez and Neito [12] used mixed interpolation tensorial component (MITC) element, enriched with drilling degree of freedom, to study free vibration

* Corresponding author.
E-mail addresses: brt.iitkgp@gmail.com (B.R. Thakur), surendraverma2501@gmail.com (S. Verma), bnsingh@aero.iitkgp.ac.in (B.N. Singh), dkmaiti@aero.iitkgp.ac.in (D.K. Maiti).

https://doi.org/10.1016/j.ast.2020.106083
1270-9638/

characteristic of folded plate. They also showed that there is no influence of drilling degree-of-freedom in membrane and bending eigen modes for flat plate. Further, Peng [13] estimated the natural frequencies of symmetric laminated folded composite plate by meshfree method using first-order shear deformation theory (FSDT). Recently, Kim and Son [14] studied the U-bend turbine structure where they optimized the structure with respect to pressure. Although, this much work has been carried out by the various researchers, all these works mentioned above deal with the isotropic folded plate structures incorporating CLPT and FSDT. However, nowadays the composite materials are widely utilized in structure for better performance. Hence, the various characteristics of composite must be incorporated in the structural analysis.

Therefore, several research works have been done on the finite element analysis of laminated composite flat plates utilizing polynomial higher order shear deformation theories (HSDT) which may be referred to the works of Reddy [15], Kant et al. [16], Bennaceur and Xu [17], and Hu et al. [18], etc. Moreover, the laminated composite flat plate has also been analyzed by many researchers using nonpolynomial shear deformation theory (NPSDT) such as Aydogdu [19], Karama et al. [20], Meiche et al. [21], Mantri et al. [22,23], Grover et al. [24], Sarangan and Singh [25], and Gupta et al. [26], etc.

Although, the flat laminated composite plate has been extensively analyzed by the several researchers, the folded laminated composite plate has been studied by very few researchers. Suresh and Malhotra [27] investigated damped free vibration analysis of composite box beams using four-noded plate finite element with FSDT, where they suggest that the loss factor due to damping follows an inverse pattern of variation with fiber angle of composite box beam. Further, Niyogi et al. [28] reported dynamic analysis of laminated composite folded plates using FSDT. Their work primarily deals with cantilever folded plate and provides a better solution than the available solution at that time. Later, Lee et al. [29] made use of Reddy's third order shear deformation theories (TSDT) to solve laminated composite folded plate problems. They suggested several measures and guidelines to use the lamination schemes and fold angle for the folded plate. Further, Lee and Wooh [30] studied the free vibration of laminated folded structure and box beam using four-noded Lagrange and Hermite finite element incorporating polynomial TSDT. They emphasized the need of employing higher-order shear deformation theory for the laminated folded and box beam structure. Then, Haldar and Sheikh [31] studied the free vibration behavior of one fold, two fold and three fold isotropic and laminated folded plate employing FSDT and FEM using shear flexible triangular element. They proposed a high-order of accuracy by the utilization of such triangular element. Later, Chun and Kassegne [32] employed FEM using TSDT to study the low-velocity impact dynamic behavior of non-prismatic laminated folded plate structures. Therein, artificial in-plane rotation is incorporated to take into account the membrane-bending coupling in folded structure, which makes eight displacement fields per node. Further, Topal and Uzman [33] carried out finite element analysis to optimize the dynamic characteristic of symmetrically laminated folded plate using modified feasible direction (MFD) method. They optimized the dynamic behavior with respect to fiber orientation in conjunction with the FSDT and concluded that the length-to-thickness ratio, crank angle, different plate length and boundary conditions significantly affect the frequency characteristic. Latter, Nayak et al. [34] developed a four noded assumed strain vortex shell element for transient analysis of initially stressed folded sandwich composite plate. In their model, displacement is approximated on the basis of FSDT having six degrees of freedom per node. It is observed that their proposed approach is able to give accurate results on the refinement of mesh density in pinched cylinder problem. Further, Le-Anh et al. [35] proposed a numerical scheme to find the optimal solution for static and free vibration analysis of folded laminated plate utilizing cell-based smoothed discrete shear gap (CS-DSG3) method in-conjunction with adjusted differential evolution (ADE) approach. They claimed to provide more accurate solution due to utilization of strain smoothing technique in CS-DSG3. Then, Nguyen-Minh et al. [36] utilized the CS-DSG3 method based on triangular element to study the static and dynamic characteristic of both unstiffened and stiffened folded plate using FSDT. Their proposed CS-FEM-DSG3 approach uses three noded triangular elements that are much easily generated for complicated geometry domain. Zhang et al. [37] studied the static analysis of folded tubes under three-point bending. They compared the traditional tubes with the folded tubes and suggested that the folded tube performs better. Recently, Thang and Hau [38] utilized FSDT layer-wise theory to analyze the static and free vibration characteristic of sandwich folded plate incorporating cell-based smoothed discrete shear gap method (CS-DSG3) and emphasized that the layer-wise gives better result than the equivalent theory in comparison with the ANSYS.

Moreover, the concept of folded structure can also be employed to the morphed winglet design and origami structure; and several works have been done in this regard. Wang et al. [39] carried out the conceptual study of a morphing winglet based on unsymmetrical stiffness. They proposed that their approach helps to reduce the requirement of the actuation system and provides a solution to the morphing skin inherently. Further, Cai et al. [40] studied the foldable origami membrane structures. They utilized the ABAQUS software to simulate the behavior of foldable membrane structure. They emphasized that the shape of membrane is an important parameter to decide the deployment of Miurarori membrane. Most recently, Varshney et al. [41] employed FSDT with finite element method in conjunction with standard deviation (SD) based technique for order of preference by similarity to ideal solution (TOPSIS) method to perform multi-response optimization of folded plate in order to rank the combination of the input parameters. To get the optimal combination of the input parameter, multi-response optimization, analysis of mean (ANOM) method is used. More recently, several research works pertaining to non-flat plate structure have been carried out by various researchers. Esposito and Gherlone [42] studied the wing box deformed-shape reconstruction based on measured strain employing iFEM. They showed that the iFEM is more accurate in reconstructing the vertical displacement of the wing box.

In the wake of extensive practical utility of folded plate structure, a more accurate and efficient solutions are required for the proper design and analysis. To achieve such efficacy, the recently developed inverse hyperbolic shear deformation theory (IHSDT), a type of nonpolynomial shear deformation theory (NPSDT) [43] is incorporated in the formulation. Moreover, the present analysis considers both pressure load as well as vertical load to incorporate more practical aspects into the problem. Further, present work considers C^0-Lagrange element through penalty approach, which is commonly used in commercial and free finite element packages. A nine noded C^0 isoparametric element with nine degrees of freedom per node is used for the modeling of folded plate to carry out the free vibration and transient analysis of folded laminated composite plate. For free vibration analysis, the subspace iteration technique [44] is adopted to extract the eigenpairs. Moreover, the effect of fold-location on the natural frequency of folded plate is also assessed to find the optimized folding location. The transient analyses are examined using unconditionally stable Newmark's time integration scheme [44]. ANSYS software finite element solution has also been obtained to compare the present solutions. As per author's knowledge, there is hardly any research paper available in the open literature which uses higher-order shear deformation theory for the free vibration and transient analysis of folded laminated composite plate. Hence, the present work provides an extensive and more accurate analysis of free vibration and transient be-

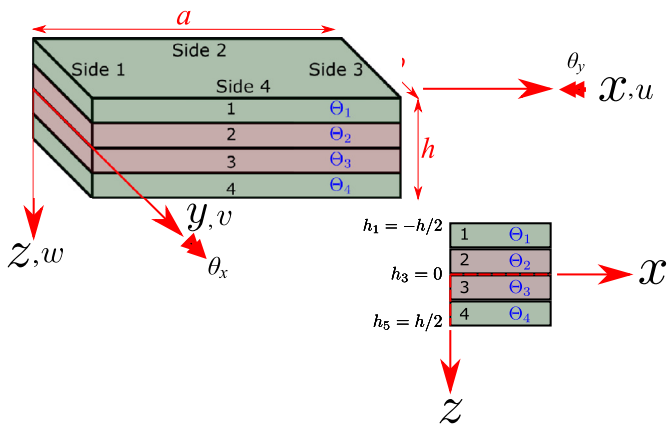

Fig. 1. Schematic diagram of laminated composite plate.

havior of folded laminated composite plate under the consideration of various structural parameter such as lamination scheme, fold angle, fold location, and boundary conditions, etc.

2. Mathematical formulation

Initially, the mathematical formulation for a flat rectangular plate is considered; and at the end, a transformation is applied to suit the folded plate formulation. A rectangular laminated composite plate of dimension $a \times b \times h$, consists of k orthotropic ply stacked in particular orientation is considered. The arrangement of these plies is represented by stacking sequence as $(\theta_1/\theta_2/\theta_3/\theta_4....)$. The schematic diagram of laminated composite plate in Cartesian coordinate system $(x-y-z)$ is shown in Fig. 1. For the mathematical formulation of the present problem of interest pertaining to folded plate, following assumptions are made-

i. Small displacement compared to the plate thickness and small strain are considered.
ii. Traction free boundary condition at the top and bottom surfaces.
iii. Thickness stretching effect has been neglected.
iv. Material properties are in elastic range.
v. Small artificial torsional stiffness has been considered.

For the consideration of displacement field model, a nonpolynomial shear deformation theory developed by Grover et al. [24] is extended to the present formulation which is expressed as follows:

$$\begin{aligned} u(x,y,z,t) &= u_0(x,y,t) - z\frac{\partial w_0}{\partial x} + f(z)\theta_x(x,y,t) \\ v(x,y,z,t) &= v_0(x,y,t) - z\frac{\partial w_0}{\partial y} + f(z)\theta_y(x,y,t) \\ w(x,y,z,t) &= w_0(x,y,t) \end{aligned} \tag{1}$$

where $f(z) = g(z) + z\Omega$, in which $g(z) = sinh^{-1}(\frac{rz}{h})$ and $\Omega = \frac{-2r}{h\sqrt{r^2+4}}$ with $r = 3$

In Eq. (1), u_0, v_0, w_0 are the mid plane displacements; θ_x, θ_y are the shear deformation at the mid plane; and h is the plate thickness. The parameter r is ascertained by the inverse method in post processing step by comparing the results of this theory with the three dimensional elasticity solutions for a wide range of problems [24]. There is presence of first order derivative of field variable in Eq. (1). Hence, it would require C^1 continuity in the field variable w_0 to carry out the finite element analysis. However, the use of Lagrange element in the finite element analysis gives utmost C^0 continuity of field variables [26]. Therefore, the reduction of C^1 to C^0 continuity is done by imposing an artificial constraint as $-\partial w_0/\partial x = \phi_x$ and $-\partial w_0/\partial y = \phi_y$ which increase the field variable from five to seven, i.e., $\boldsymbol{u} = \{u_0,\ v_0,\ w_0,\ \phi_x,\ \phi_y,\ \theta_x,\ \theta_y\}^T$. The effect of artificial constraints is severe when the plate is thick $(a/h < 10)$. Thus, to model the plate properly, the penalty approach has been considered which has not been reported for the analysis of folded plate in the literature, as most of the work have used the Hermite interpolation for transverse deflection. Other than the penalty approach, the C^1 continuity, alternatively, can be modeled by Hermite element in the formulation, which is rarely used in commercial and free FE packages for practical application.

Further, the state-of-strain, $\{\epsilon\}$ at a point corresponding to modified displacement field, in the Cartesian coordinate $(x-y-z)$, is expressed as

$$\boldsymbol{\epsilon} = \begin{Bmatrix} \frac{\partial u}{\partial x} \\ \frac{\partial v}{\partial y} \\ \frac{\partial u}{\partial y} + \frac{\partial v}{\partial x} \\ \frac{\partial v}{\partial z} + \frac{\partial w}{\partial y} \\ \frac{\partial u}{\partial z} + \frac{\partial w}{\partial x} \end{Bmatrix} = \begin{bmatrix} \frac{\partial}{\partial x} & 0 & 0 & z\frac{\partial}{\partial x} & 0 & f(z)\frac{\partial}{\partial x} & 0 \\ 0 & \frac{\partial}{\partial y} & 0 & 0 & z\frac{\partial}{\partial y} & 0 & f(z)\frac{\partial}{\partial y} \\ \frac{\partial}{\partial y} & \frac{\partial}{\partial x} & 0 & z\frac{\partial}{\partial y} & z\frac{\partial}{\partial x} & f(z)\frac{\partial}{\partial y} & f(z)\frac{\partial}{\partial x} \\ 0 & 0 & \frac{\partial}{\partial y} & 0 & 1 & 0 & f'(z) \\ 0 & 0 & \frac{\partial}{\partial x} & 1 & 0 & f'(z) & 0 \end{bmatrix} \begin{Bmatrix} u_0 \\ v_0 \\ w_0 \\ \phi_x \\ \phi_y \\ \theta_x \\ \theta_y \end{Bmatrix} \tag{2}$$

The strain vector, ($\boldsymbol{\epsilon}$) can be written in terms of in-plane strain vector, $\boldsymbol{\epsilon_b} = [\epsilon_{xx}\, \epsilon_{yy}\, \gamma_{xy}]^T = \boldsymbol{\epsilon_{b1}} + z\boldsymbol{\epsilon_{b2}} + f(z)\boldsymbol{\epsilon_{b3}}$ and transverse shear strain vector, $\boldsymbol{\epsilon_s} = [\gamma_{yz}\, \gamma_{yz}]^T = \boldsymbol{\epsilon_{s1}} + f'(z)\boldsymbol{\epsilon_{s2}}$ as

$$\{\boldsymbol{\epsilon}\} = \begin{Bmatrix} \boldsymbol{\epsilon_b} \\ \boldsymbol{\epsilon_s} \end{Bmatrix}, \{\boldsymbol{\epsilon_b}\} = \begin{Bmatrix} \frac{\partial u}{\partial x} \\ \frac{\partial v}{\partial y} \\ \frac{\partial u}{\partial y} + \frac{\partial v}{\partial x} \end{Bmatrix}, \{\boldsymbol{\epsilon_s}\} = \begin{Bmatrix} \frac{\partial v}{\partial z} + \frac{\partial w}{\partial y} \\ \frac{\partial u}{\partial z} + \frac{\partial w}{\partial x} \end{Bmatrix}$$

The constitutive equations for an arbitrary k^{th} orthotropic layer in global coordinate for plane stress problem are given by the following relation [45].

$$\{\boldsymbol{\sigma}\}^{(k)} = [\,\bar{\mathbf{Q}}\,]^{(k)}\{\boldsymbol{\epsilon}\}^{(k)} \tag{3}$$

where, $\{\boldsymbol{\sigma}\}$, $\{\boldsymbol{\epsilon}\}$, and $[\,\bar{\mathbf{Q}}\,]$ are stress vector, strain vector, and the material matrix in the global coordinate, respectively. The detail expression can be found in standard FE text book [45].

Further, to obtain the equations of motion, Hamilton's principle is employed for the arbitrary variable and admissible virtual displacement $\delta\{u\,, v\,, w\}$ and the same is written as

$$\delta \int_{t_i}^{t_f} \mathcal{L} dt = \int_{t_i}^{t_f} \left(\delta\mathcal{K} - \delta\mathcal{U} - \delta\mathcal{U}_\gamma + \delta\mathcal{W}_{ext}\right) dt = 0 \tag{4}$$

Strain energy The strain energy due to mechanical strain for plate is expressed as,

$$\delta\mathcal{U} = \sum_{k=1}^{n} \left(\int_\Omega (\sigma_{xx}^k \delta\epsilon_{xx}^k + \sigma_{yy}^k \delta\epsilon_{yy}^k + \sigma_{xy}^k \delta\gamma_{xy}^k + \sigma_{yz}^k \delta\gamma_{yz}^k + \sigma_{xz}^k \delta\gamma_{xz}^k) d\Omega \right) \tag{5}$$

Kinetic energy The kinetic energy of the flat plate is expressed as follows,

$$\int_{t_i}^{t_f} \delta\mathcal{K} dt = -\int_{t_i}^{t_f} \sum_{k=1}^{n} \left[\int_\Omega \delta\{\boldsymbol{u}\}\, \rho^k \{\ddot{\boldsymbol{u}}\}\, d\Omega \right] dt \tag{6}$$

Work done The potential energy of the system due to mechanical loading is written as

$$\delta\mathcal{W}_{ext} = \int_A (\delta u P_u + \delta v P_v + \delta w P_w)\, dA \tag{7}$$

where P_u, P_v, P_w are the load components of applied load, P in the u, v, and w direction, respectively.

2.1. Finite element discretization

A nine noded isoparametric element with seven degrees of freedom (DOFs) $(u_0, v_0, w_0, \phi_x, \phi_y, \theta_x, \theta_y)$ per node is employed for the inverse hyperbolic shear deformation theory (IHSDT) based finite element (FE) formulation. The present finite element utilizes a set of Lagrange interpolation function, N_i corresponding to each node. And using these interpolation functions, a generalized field variables, $\{\boldsymbol{u}\}$ and geometric point, (x, y) within the element are obtained from nodal fields variable and nodal geometric description as

$$\{\boldsymbol{u}\} = \sum_{i=1}^{9} N_i \{\boldsymbol{q}\}_i, \quad x = \sum_{i=1}^{9} N_i x_i, \quad y = \sum_{i=1}^{9} N_i y_i \tag{8}$$

Where, $\{\boldsymbol{q}\}_i$ is the corresponding nodal field variables associated with i^{th} node, and x_i and y_i are the co-ordinate values of the corresponding i^{th} node.

Knowing the generalized displacement vector, $\boldsymbol{u}$ at all points within the element, one can express the generalized strain vector, $\boldsymbol{\epsilon_b}$ and $\boldsymbol{\epsilon_s}$ at any point as

$$\boldsymbol{\epsilon_b} = \boldsymbol{B_b q} = \sum_{i=1}^{n} \begin{bmatrix} \frac{\partial N_i}{\partial x} & 0 & 0 & 0 & 0 & 0 & 0 \\ 0 & \frac{\partial N_i}{\partial y} & 0 & 0 & 0 & 0 & 0 \\ \frac{\partial N_i}{\partial y} & \frac{\partial N_i}{\partial x} & 0 & 0 & 0 & 0 & 0 \\ 0 & 0 & 0 & \frac{\partial N_i}{\partial x} & 0 & 0 & 0 \\ 0 & 0 & 0 & 0 & \frac{\partial N_i}{\partial y} & 0 & 0 \\ 0 & 0 & 0 & \frac{\partial N_i}{\partial y} & \frac{\partial N_i}{\partial x} & 0 & 0 \\ 0 & 0 & 0 & 0 & 0 & \frac{\partial N_i}{\partial x} & 0 \\ 0 & 0 & 0 & 0 & 0 & 0 & \frac{\partial N_i}{\partial y} \\ 0 & 0 & 0 & 0 & 0 & \frac{\partial N_i}{\partial y} & \frac{\partial N_i}{\partial x} \end{bmatrix} \begin{Bmatrix} u_{0i} \\ v_{0i} \\ w_{0i} \\ \phi_{xi} \\ \phi_{yi} \\ \theta_{xi} \\ \theta_{yi} \end{Bmatrix} \tag{9}$$

and

$$\boldsymbol{\epsilon_s} = \boldsymbol{B_s q} = \sum_{i=1}^{n} \begin{bmatrix} 0 & 0 & \frac{\partial N_i}{\partial y} & 0 & N_i & 0 & 0 \\ 0 & 0 & \frac{\partial N_i}{\partial x} & N_i & 0 & 0 & 0 \\ 0 & 0 & 0 & 0 & 0 & 0 & N_i \\ 0 & 0 & 0 & 0 & 0 & N_i & 0 \end{bmatrix} \begin{Bmatrix} u_{0i} \\ v_{0i} \\ w_{0i} \\ \phi_{xi} \\ \phi_{yi} \\ \theta_{xi} \\ \theta_{yi} \end{Bmatrix} \tag{10}$$

in which

$$\{\boldsymbol{q}\} = \begin{Bmatrix} \boldsymbol{q}_1^T & \boldsymbol{q}_2^T & \dots & \boldsymbol{q}_8^T & \boldsymbol{q}_9^T \end{Bmatrix}^T \qquad \boldsymbol{q}_i = \begin{Bmatrix} u_{0i} & v_{0i} & w_{0i} & \phi_{xi} & \phi_{yi} & \theta_{xi} & \theta_{yi} \end{Bmatrix}^T$$

and

$$\boldsymbol{\epsilon_b} = \begin{Bmatrix} \frac{\partial u_0}{\partial x} \\ \frac{\partial v_0}{\partial y} \\ \frac{\partial u_0}{\partial y} + \frac{\partial v_0}{\partial x} \\ \frac{\partial \phi_x}{\partial x} \\ \frac{\partial \phi_y}{\partial y} \\ \frac{\partial \phi_x}{\partial y} + \frac{\partial \phi_y}{\partial x} \\ \frac{\partial \theta_x}{\partial x} \\ \frac{\partial \theta_y}{\partial y} \\ \frac{\partial \theta_x}{\partial y} + \frac{\partial \theta_y}{\partial x} \end{Bmatrix} \quad \textit{and} \quad \boldsymbol{\epsilon_s} = \begin{Bmatrix} \frac{\partial w_0}{\partial y} + \phi_y \\ \frac{\partial w_0}{\partial x} + \phi_x \\ \theta_y \\ \theta_x \end{Bmatrix}$$

The force resultants are given by the following expression as

$$[N_x\, N_y\, N_{xy}\, M_x\, M_y\, M_{xy}\, P_x\, P_y\, P_{xy}]^T = [\boldsymbol{D_b}]\{\boldsymbol{\epsilon_b}\} \tag{11}$$

$$[N_{yz}\, N_{xz}\, M_{yz}\, M_{xz}]^T = [\boldsymbol{D_s}]\{\boldsymbol{\epsilon_s}\} \tag{12}$$

where the material matrix $[\boldsymbol{D_b}]$ and $[\boldsymbol{D_s}]$ of the composite plate is given by

$$[\boldsymbol{D_b}] = \begin{bmatrix} \boldsymbol{A} & \boldsymbol{B} & \boldsymbol{C} \\ \boldsymbol{B} & \boldsymbol{D} & \boldsymbol{E} \\ \boldsymbol{C} & \boldsymbol{E} & \boldsymbol{F} \end{bmatrix} \text{ and } [\boldsymbol{D_s}] = \begin{bmatrix} \boldsymbol{A_s} & \boldsymbol{B_s} \\ \boldsymbol{B_s} & \boldsymbol{C_s} \end{bmatrix}$$

Where

$$\begin{bmatrix} \boldsymbol{A} & \boldsymbol{B} & \boldsymbol{C} & \boldsymbol{D} & \boldsymbol{E} & \boldsymbol{F} \end{bmatrix} = \int_{-h/2}^{h/2} \begin{bmatrix} 1 & z & f(z) & z^2 & zf(z) & f(z)^2 \end{bmatrix} \bar{\boldsymbol{Q}}_{\boldsymbol{ij}} dz \quad i, j = 1, 2, 6 \tag{13}$$

$$\begin{bmatrix} \boldsymbol{A_s} & \boldsymbol{B_s} & \boldsymbol{C_s} \end{bmatrix} = \int_{-h/2}^{h/2} \begin{bmatrix} 1 & f_{,z}(z) & (f_{,z}(z))^2 \end{bmatrix} \bar{\boldsymbol{Q}}_{\boldsymbol{ij}} dz \quad i, j = 4, 5 \tag{14}$$

Stiffness matrix The elemental stiffness matrix of the laminate for the finite element method is given by

$$\boldsymbol{K_e} = \int [\boldsymbol{B_b}]^T [\boldsymbol{D_b}][\boldsymbol{B_b}] dA + \int [\boldsymbol{B_s}]^T [\boldsymbol{D_s}][\boldsymbol{B_s}] dA \tag{15}$$

The strain energy pertaining to artificial constraints which is raised due to the conversion of C^1-continuity to C^0-continuity, can be expressed in terms of penalty parameter, γ as

$$\boldsymbol{U_\gamma} = \frac{\gamma}{2} \int_V \left\{ \left(\phi_x + \frac{\partial w_0}{\partial x} \right)^2 + \left(\phi_y + \frac{\partial w_0}{\partial y} \right)^2 \right\} dV \tag{16}$$

Similar to strain-displacement matrix, the artificial constraints can be expressed as

$$\left(\phi_x + \frac{\partial w_0}{\partial x} \right) = [\boldsymbol{P_1}]\{\boldsymbol{q}\}; \left(\phi_y + \frac{\partial w_0}{\partial y} \right) = [\boldsymbol{P_2}]\{\boldsymbol{q}\} \tag{17}$$

Now, using above conditions, penalty strain energy can be rewritten as

$$\boldsymbol{U_\gamma} = \frac{\gamma}{2}\int_V \left\{ \{\boldsymbol{q}\}^T [\boldsymbol{P_1}]^T [\boldsymbol{P_1}] \{\boldsymbol{q}\} + \{\boldsymbol{q}\}^T [\boldsymbol{P_2}]^T [\boldsymbol{P_2}] \{\boldsymbol{q}\} \right\} dV \tag{18}$$

The selection of penalty parameter plays an important role in avoiding the ill-conditioning of the stiffness matrix and ensuring the accuracy of the analysis. Generally, penalty is taken to be as large as possible and compatible with the computer hardware architecture for software implementation. However, in this analysis penalty parameter is taken as 10^8.

The stiffness matrix due to artificial constraints can be written as

$$\boldsymbol{K_\gamma} = \int_A \left([\boldsymbol{P_1}]^T [\boldsymbol{P_1}] + [\boldsymbol{P_2}]^T [\boldsymbol{P_2}] \right) dA \tag{19}$$

Total stiffness matrix of an element is

$$\boldsymbol{K} = \boldsymbol{K_e} + \gamma \boldsymbol{K_\gamma}$$

Mass matrix $[\boldsymbol{M}] = \int_A \{\mathbb{R}\}^T [\bar{m}] \{\mathbb{R}\} dA$

$$[\bar{m}] = \sum_{k=1}^{n} \int_{z_k}^{z_{k+1}} \rho^k \begin{bmatrix} 1 & 0 & 0 & z & 0 & f(z) & 0 \\ 0 & 1 & 0 & 0 & z & 0 & f(z) \\ 0 & 0 & 1 & 0 & 0 & 0 & 0 \\ z & 0 & 0 & z^2 & 0 & zf(z) & 0 \\ 0 & z & 0 & 0 & z^2 & 0 & zf(z) \\ f(z) & 0 & 0 & zf(z) & 0 & f(z)^2 & 0 \\ 0 & f(z) & 0 & 0 & zf(z) & 0 & f(z)^2 \end{bmatrix} dz$$

$$\mathbb{R} = \sum_{i=1}^{N} \begin{bmatrix} N_i & 0 & 0 & 0 & 0 & 0 & 0 \\ 0 & N_i & 0 & 0 & 0 & 0 & 0 \\ 0 & 0 & N_i & 0 & 0 & 0 & 0 \\ 0 & 0 & 0 & N_i & 0 & 0 & 0 \\ 0 & 0 & 0 & 0 & N_i & 0 & 0 \\ 0 & 0 & 0 & 0 & 0 & N_i & 0 \\ 0 & 0 & 0 & 0 & 0 & 0 & N_i \end{bmatrix}$$

Elemental load vector $\boldsymbol{F}_m = \int \boldsymbol{W}^T P dA$

$$\boldsymbol{W} = \begin{Bmatrix} \boldsymbol{W}_1 & \boldsymbol{W}_2 & \boldsymbol{W}_3 & \boldsymbol{W}_4 & \boldsymbol{W}_5 & \boldsymbol{W}_6 & \boldsymbol{W}_7 & \boldsymbol{W}_8 & \boldsymbol{W}_9 \end{Bmatrix}$$

$$\boldsymbol{W}_i = \begin{bmatrix} N_i cos(x, Z^*) & N_i cos(y, Z^*) & N_i cos(z, Z^*) & 0 & 0 & 0 & 0 \end{bmatrix} \quad i = 1, \cdots, 9$$

where Z^* is the applied force direction. In case of vertical load, the force direction, Z^* is equivalent to global Z direction. Whereas, in case of pressure load; Z^* is equivalent to local z direction.

Governing equation The governing equations of the laminated composite plate can be written as

For free vibration analysis (or eigen value problem)

$$[\boldsymbol{M}] \{\ddot{\boldsymbol{q}}\} + [\boldsymbol{K}] \{\boldsymbol{q}\} = 0 \tag{20}$$

For transient analysis (or initial value problem)

$$[\boldsymbol{M}] \{\ddot{\boldsymbol{q}}\} + [\boldsymbol{K}] \{\boldsymbol{q}\} = \{\boldsymbol{F}_m\} \tag{21}$$

Where $\boldsymbol{K}$, $\boldsymbol{M}$ and $\boldsymbol{F}_m$ are the global stiffness, mass matrices, and force vector respectively.

2.2. Folded plate formulation

Now, for the folded plate formulation, a one-fold and two-fold geometries are considered as shown in Fig. 2. First of all, the elemental matrices are calculated on the basis of seven degrees of freedom (i.e., u_0, v_0, w_0, ϕ_x, ϕ_y, θ_x, θ_y). Then, to incorporate the folded plate formulation, two drilling degree of freedom, ϕ_z and θ_z are introduced and the elemental matrices are blown to the nine degrees of freedom per node before assembly. A very small value (1000 times less than the smallest diagonal value) is taken for the diagonal elemental matrices corresponding to the drilling degree of freedom [46]. Afterwards, a transformation is performed to convert the local degrees of freedom to global degrees of freedom by following approach.

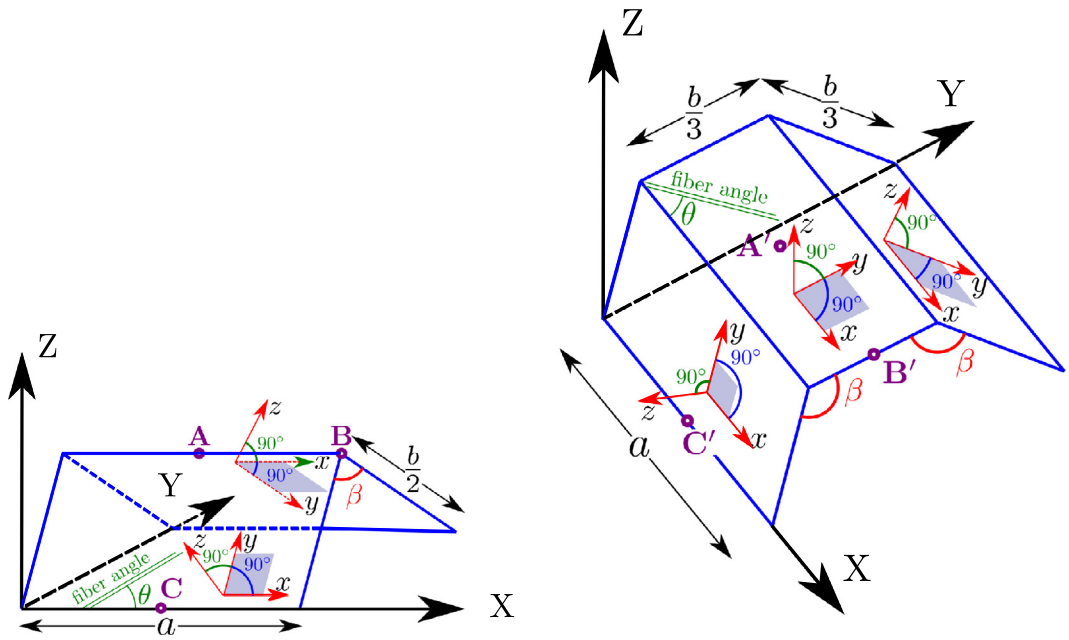

(a) One-fold folded plate. (b) Two-fold folded plate.

Fig. 2. Schematic diagram of two-fold folded cantilever plate with fold angle β.

$$\begin{Bmatrix} u_0 \\ v_0 \\ w_0 \\ \phi_x \\ \phi_y \\ \phi_z \\ \theta_x \\ \theta_y \\ \theta_z \end{Bmatrix} = \begin{bmatrix} C(x,X) & C(x,Y) & C(x,Z) & 0 & 0 & 0 & 0 & 0 & 0 \\ C(y,X) & C(y,Y) & C(y,Z) & 0 & 0 & 0 & 0 & 0 & 0 \\ C(z,X) & C(z,Y) & C(z,Z) & 0 & 0 & 0 & 0 & 0 & 0 \\ 0 & 0 & 0 & C(y,Y) & -C(y,X) & C(y,Z) & 0 & 0 & 0 \\ 0 & 0 & 0 & -C(x,Y) & C(x,X) & -C(x,Z) & 0 & 0 & 0 \\ 0 & 0 & 0 & C(z,Y) & -C(z,X) & C(z,Z) & 0 & 0 & 0 \\ 0 & 0 & 0 & 0 & 0 & 0 & C(y,Y) & -C(y,X) & C(y,Z) \\ 0 & 0 & 0 & 0 & 0 & 0 & -C(x,Y) & C(x,X) & -C(x,Z) \\ 0 & 0 & 0 & 0 & 0 & 0 & C(z,Y) & -C(z,X) & C(z,Z) \end{bmatrix} \begin{Bmatrix} u_0' \\ v_0' \\ w_0' \\ \phi_X' \\ \phi_Y' \\ \phi_Z' \\ \theta_X' \\ \theta_Y' \\ \theta_Z' \end{Bmatrix} \tag{22}$$

where $C(x, X)$ represents the cosine of the angle between local x and global X. In brief, the above equation can be written as

$$\{\boldsymbol{u}\} = [\boldsymbol{T}]\{\boldsymbol{u}'\} \tag{23}$$

where the element of transformation matrix, $[\boldsymbol{T}]$ are the direction cosines between the global and local coordinates. The global coordinate field variables are denoted by the prime notation. After imposing the transformation, the global stiffness matrix, mass matrix, and force vector are expressed as

$$[\bar{\boldsymbol{K}}] = [\bar{\boldsymbol{T}}]^T[\boldsymbol{K}][\bar{\boldsymbol{T}}] \tag{24}$$

$$[\bar{\boldsymbol{M}}] = [\bar{\boldsymbol{T}}]^T[\boldsymbol{M}][\bar{\boldsymbol{T}}] \tag{25}$$

$$\{\bar{\boldsymbol{F}}_{\boldsymbol{m}}\} = [\bar{\boldsymbol{T}}]^T\{\boldsymbol{F}_{\boldsymbol{m}}\} \tag{26}$$

where $[\bar{\boldsymbol{T}}]$ is given as follows

$$[\bar{\boldsymbol{T}}] = \begin{bmatrix} [\boldsymbol{T}] & & \\ & \ddots & \\ & & [\boldsymbol{T}] \end{bmatrix} \quad 9\,\text{times} \tag{27}$$

Now the governing equations for the free and forced vibration problem are stated as

$$[\bar{\boldsymbol{M}}]\ddot{\boldsymbol{q}}' + [\bar{\boldsymbol{K}}]\{\boldsymbol{q}'\} = 0 \tag{28}$$

and

$$[\bar{\boldsymbol{M}}]\ddot{\boldsymbol{q}}' + [\bar{\boldsymbol{K}}]\{\boldsymbol{q}'\} = \{\bar{\boldsymbol{F}}_{\boldsymbol{m}}(\boldsymbol{t})\} \tag{29}$$

where $\ddot{\boldsymbol{q}}'$ and $\boldsymbol{q}'$ are the acceleration and displacement vector of the folded plate. $\bar{\boldsymbol{F}}_{\boldsymbol{m}}(\boldsymbol{t})$ is the transverse load applied at the surface of the plate.

3. Result and discussion

In this section, various examples have been taken to perform the free vibration and forced vibration analysis of isotropic and laminated composite folded plate. Both, the one-fold and two-fold plates with various combinations of boundary conditions are considered for the numerical analysis. A detailed solution and discussions are presented for the better understanding of design and analysis of folded plate structure.

3.1. Material properties

Material properties used for the analysis are as follows.

1. Material MM1 [28]: $E = 10.92 \times 10^9$ N/m^2, $\nu = 0.3$, $\rho = 1000$ kg/m^3
2. Material MM2 [28]: $E_1 = 60.7 \times 10^9$ N/m^2, $E_2 = 24.8 \times 10^9$ N/m^2, $G_{12} = G_{13} = G_{23} = 12.0 \times 10^9$ N/m^2, $\nu_{12} = \nu_{21} = 0.23$, $\rho = 1300$ kg/m^3

3.2. Boundary condition

Several combinations of clamped and free boundary conditions have been used in the present work and the conditions for the same are mentioned below. The boundary convention has been accepted as, if $'ABCD'$ is the boundary condition then $'A'$ is employed over the edge along $X = 0$, $'B'$ is on the edge $Y = 0$, $'C'$ is on the edge $X = a$, and $'D'$ is employed over the edge $Y = b$.

- Clamped (C) boundary condition:
  $u'_0 = v'_0 = w'_0 = \phi'_x = \phi'_y = \phi'_z = \theta'_x = \theta'_y = \theta'_z = 0$
- Simply supported (S) boundary condition:
  $v'_0 = w'_0 = \phi'_y = \phi'_z = \theta'_y = \theta'_z = 0$ at $X = 0$ and $X = a$,
  $u'_0 = w'_0 = \phi'_x = \phi'_z = \theta'_x = \theta'_z = 0$ at $Y = 0$ and $Y = b$
- Free (F) boundary condition:
  $(u'_0,\ v'_0,\ w'_0,\ \phi'_x,\ \phi'_y,\ \phi'_z,\ \theta'_x,\ \theta'_y,\ \theta'_z) \neq 0$, i.e., no prescribed boundary conditions.

3.3. Free vibration analysis

In this section, free vibration of folded laminated composite plate utilizing inverse hyperbolic shear deformation theory has been analyzed. The present formulation has been extensively validated from the available literature and the obtained ANSYS software solution, then the new results have been presented. The non-dimentionalized fundamental frequency is given by $\bar{\omega} = (\omega a)\sqrt{\rho(1-\nu_{12}^2)/E_1}$. The solution has been obtained for various combinations of clamped, free, and simply supported boundary conditions.

3.3.1. Free vibration of one-fold folded isotropic plate

An isotropic one-fold cantilever (CFFF) square plate is considered for the free vibration analysis which resembles the geometry as shown in Fig. 2a. The material properties of the plate are MM1 and have side-length $a = b = 1.5$ m with side-to-thickness ratio, $a/h = 50$. The first five natural frequencies have been obtained for the various crank angles and shown in Table 1. The obtained results have been compared and validated with the available solutions in the literature and are found to be in good agreement. Since, the present formulation utilizes higher order nonpolynomial shear deformation theory, the obtained solutions are found to be better than the other available solutions as observed in Table 1, because FSDT and CPT solution over-predict the natural frequencies. It is also observed from the Table 1 that the difference between the first natural frequency of flat plate (crank angle=180^0) and the folded plate is significant, whereas the first natural frequency is found to be almost equal for any other crank angle (not equal to 180^0). This observation suggests that the fold in the plate increases the stiffness of the plate due to participation of in-plane stiffness into bending stiffness. Moreover, the mode shapes of cantilever folded plate corresponding to first three modes are also shown in Fig. 3 which shows the mode shape for the crank angle, $\beta = 90^0$ and $\beta = 120^0$. Due to the effect of folding angles, a lot of difference in the mode shape can be observed for the two crank angle, however, the difference in the modal frequencies is not much.

Further, the same problem is analyzed for the clamped-clamped (CFCF, folded side clamped) boundary condition and the obtained non-dimensional natural frequencies for side-to-thickness ratio $a/h = 10, 100$ and the crank angle $\beta = 90^0, 120^0, 150^0$ are shown in the Table 2. It is observed that for the CFCF boundary condition, the natural frequencies of thin plate ($a/h = 100$) are almost same for different crank angle, whereas for the thick plate ($a/h = 10$), the natural frequencies are different for various crank angle because of prominent extensional stiffness contribution in thick plate.

3.3.2. Free vibration of two-fold folded isotropic plate

Here, a two-fold folded square isotropic plate as shown in Fig. 2b has been analyzed and the first five natural frequencies are shown in Table 3 for fold angle 90^0, 120^0 and 150^0. The plate is made of material MM1 and has side-length as $a = b = 2$ m with $a/h = 50$. The obtained solutions are compared with the available results in the literature and found to be performing better than the available one due to the IHSDT theory used in the formulation, as the obtained non-dimensional natural frequencies are less than the available FSDT results of Niyogi et al. [28] and CPT solution of Liu et al. [8] which over predict the frequency. Moreover, it is observed that, unlike the one-fold solution, in the two-fold plate the first natural frequency various fold angle is significantly different due to prominent bending-extensional

Table 1
Nondimensional natural frequency of cantilever isotropic single-folded square plate.

Crank angle	Mode number	$\bar{\omega} = \omega a\sqrt{\rho(1-\nu^2)/E}$			
		Present	Niyogi et al. [28]	Liu et al. [8]	Irie et al. [2]
90^0	1	0.0485	0.049	0.0491	0.0492
	2	0.0968	0.0971	0.0971	0.0977
	3	0.1765	0.1881	0.1786	0.1794
	4	0.2070	0.2183	0.2084	0.2101
	5	0.3450	0.3505	0.3558	0.3573
120^0	1	0.0486	0.049	0.0491	0.0492
	2	0.0938	0.0941	0.0943	0.0949
	3	0.1766	0.1883	0.1787	0.1795
	4	0.2051	0.216	0.2065	0.2082
	5	0.2885	0.293	0.2971	0.2984
150	1	0.0486	0.0491	0.0491	0.0492
	2	0.0800	0.0804	0.0812	0.0816
	3	0.1767	0.1883	0.1787	0.1795
	4	0.1886	0.1942	0.1912	0.1927
	5	0.2175	0.2256	0.2210	0.2227
180^0	1	0.0200	0.0200	0.0200	0.0201
	2	0.0488	0.0489	0.0492	0.0493
	3	0.1225	0.1230	0.1235	0.1234
	4	0.1563	0.1567	0.1566	0.2577
	5	0.1773	0.1784	0.1787	0.1796

Table 2
Nondimensional natural frequency ($\bar{\omega}$) of isotropic single-folded plate under CFCF boundary condition.

Crank angle	Source	a/h	$\bar{\omega} = \omega a\sqrt{\rho(1-\nu^2)/E}$				
			Mode 1	Mode 2	Mode 3	Mode 4	Mode 5
150^0	Present	100	0.0761	0.0891	0.1944	0.2022	0.2292
	Mohammadi et al. [47]		0.0762	0.0893	0.1937	0.2017	0.2301
	Harnadez and Hervella [12]		0.0763	0.0893	0.1946	0.2026	0.2307
120^0	Present		0.0761	0.0894	0.1945	0.2026	0.2291
90^0	Present		0.0761	0.0895	0.1945	0.2027	0.2290
150^0	Present	10	0.6661	0.6895	1.1658	1.5992	1.6529
	Harnadez and Hervella [12]		0.6668	0.6931	1.1663	1.5953	1.6525
120^0	Present		0.6886	0.7478	1.2805	1.6158	1.6514
90^0	Present		0.6864	0.7859	1.3898	1.5136	1.6476

coupling in the two-fold folded plate. This observation suggests that the stiffness of two-fold folded plate is more susceptible to crank angle than the one-fold folded plate. Further, in the case of two-fold folded isotropic plate, as the results are shown in Table 3, the first natural frequency decreases with increase in the fold angle, which reveals that as the fold angle increases in the two-fold plate, the plate becomes less stiff due to decrease in flexural rigidity. Moreover, the first three mode shape for two-fold folded isotropic cantilever plate corresponding to crank angle $\beta = 90^0$ and $\beta = 120^0$ have also been shown in Fig. 4. The observed mode shapes are enormously complex and distinct for both the crank angles due to the effect of folding.

Further, the same problem is analyzed for the CFCF boundary condition and obtained solutions are shown in the Table 4. It is observed that the natural frequency decreases with increase in side-to-thickness ratio, a/h. Also, the non-dimensional natural frequency is found to be decreasing with increase in crank angle for the CFCF boundary condition. It is also observed that the natural frequency under CFCF boundary condition is more than the CFFF boundary condition due to more boundary constraints in the CFCF boundary condition.

Moreover, an isotropic plate as mentioned in Haldar and Sheikh [31] is considered for validation of simply supported boundary condition where SFCF (one of the folded sides simply supported at $X = 0$) boundary condition is considered. The obtained solution is shown in Table 5. It is observed that the present solutions are not only in well agreement with the available one but also predicting in a better way due to utilization of higher-order NPSDT.

3.3.3. Free vibration of one-fold folded laminated composite plate

In this section, the single folded laminated composite plates are analyzed for various fold angle, lamination schemes, and boundary conditions. The material properties used for the composite plate are MM2 with side-to-thickness ratio, $a/h = 50$. The one-fold cantilever (CFFF) plate having $a = b = 1.5$ m is considered for the evaluation of non-dimensional natural frequencies. The obtained solutions for the one-fold folded plate are shown in Table 6. It is observed that for the three-layered one-fold folded laminated composite plate, the first natural frequencies are found to be almost same for different crank angle except the 180^0 (flat plate) where the first natural frequencies are found to be significantly different than the other crank angle. This is because, the fold in the plate increases the flexural rigidity of plate due to participation of in-plane stiffness, hence increases the stiffness of plate. It can also be observed that as the fiber-orientation angle (θ) increases in the three-layered lamination scheme $[\theta/-\theta/\theta]$, the first natural frequency decreases for a particular crank angle due to decrease in the stiffness. Further, a one-fold folded cross-ply $[0^0/90^0/0^0]$ and angle-ply $[45^0/-45^0/45^0]$ laminated composite plate are analyzed for the free vibration under the clamped-clamped (CFCF) boundary condition and the obtained natural frequencies are presented in Table 7. It is observed from Table 7 that for a particular lamination scheme and crank angle, the first natural frequency decreases

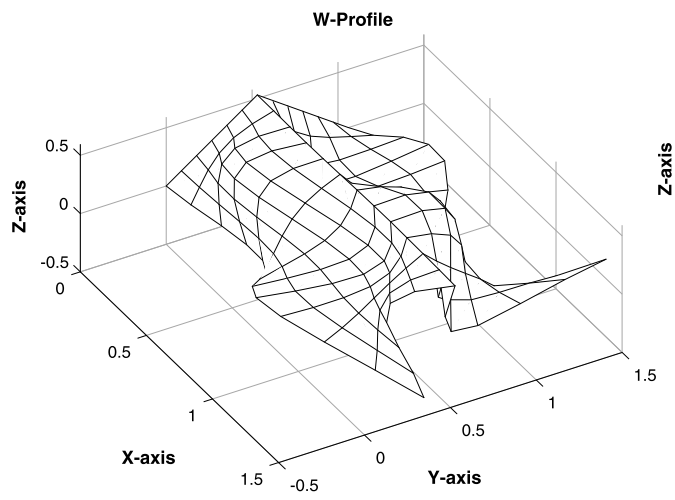

Mode 1, $\beta = 90$.

Mode 1, $\beta = 120$.

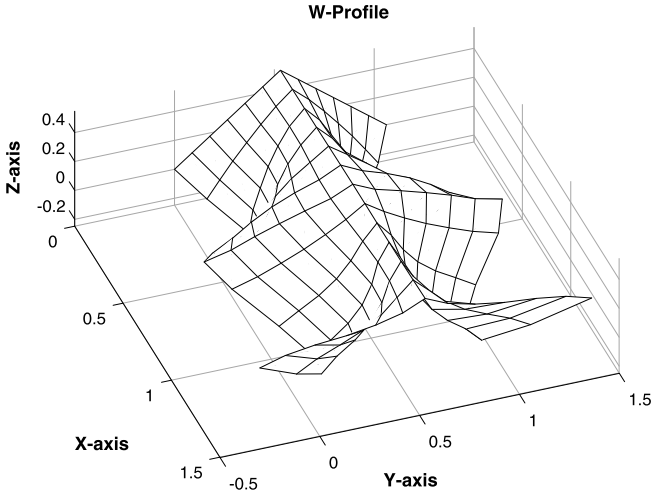

Mode 2, $\beta = 90$.

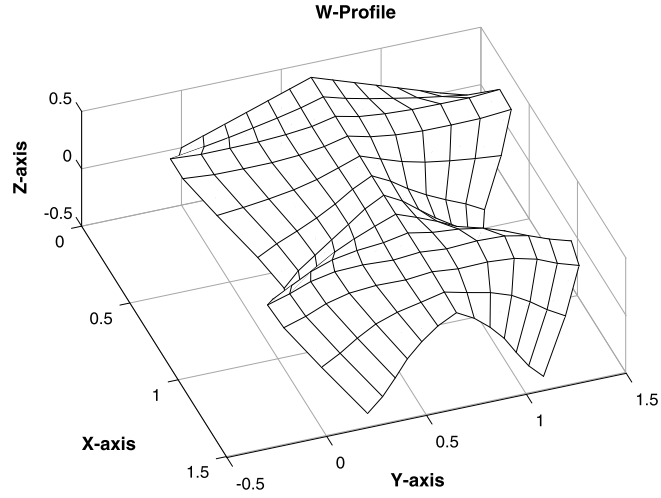

Mode 2, $\beta = 120$.

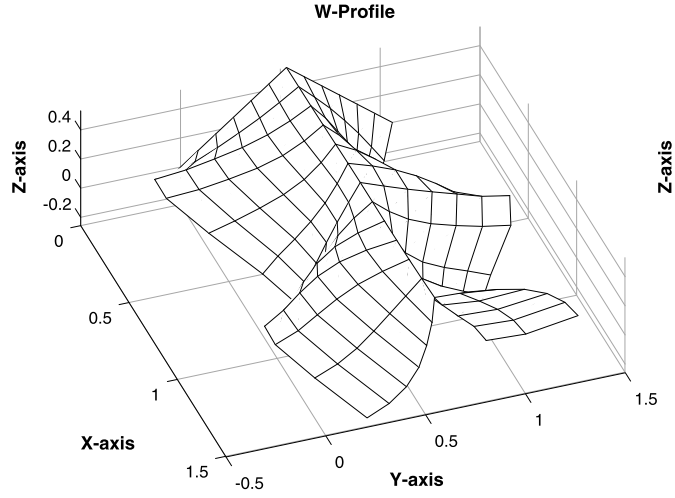

Mode 3, $\beta = 90$.

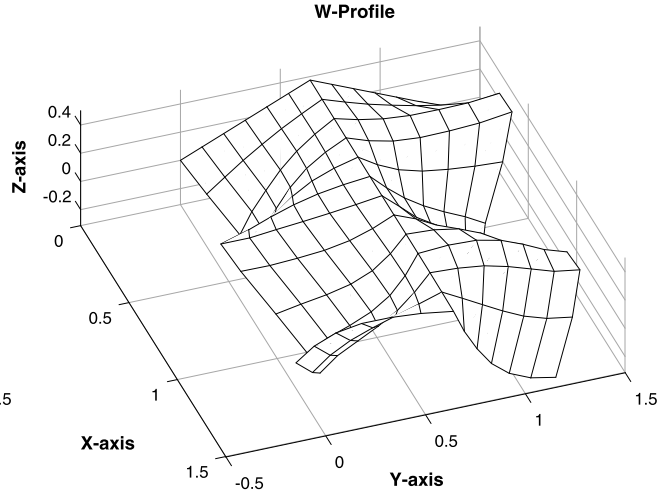

Mode 3, $\beta = 120$.

Fig. 3. Modal shape corresponding to first three modes of one-fold cantilever isotropic plate for crank angle 90^0 and 120^0.

with increase in side-to-thickness ratio. Moreover, the first natural frequency of $[0^0/90^0/0^0]$ is found to be more than the corresponding frequency of $[45^0/-45^0/45^0]$ lamination scheme.

Further, the same problem is also analyzed with ANSYS software for CFFF and CFCF boundary conditions and the obtained solutions are shown in Table 8. The solutions obtained with ANSYS software are in well agreement with the present computed result with MATLAB finite element code as shown in Tables 6 and 7. There are some discrepancies found due to utilization of FSDT in the ANSYS software.

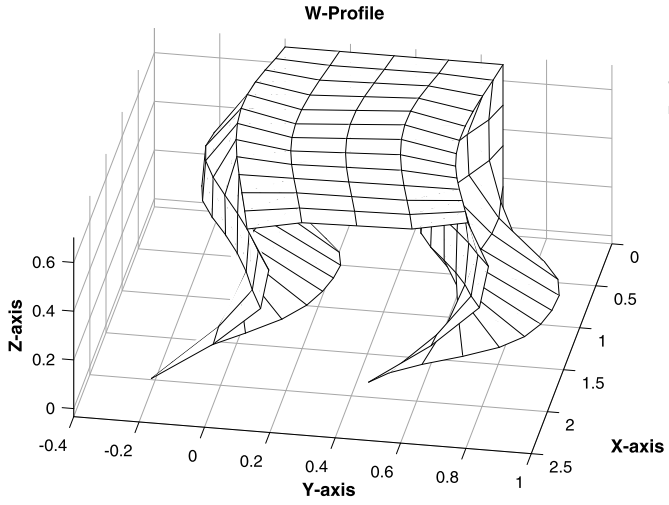

Mode 1, $\beta = 90^0$.

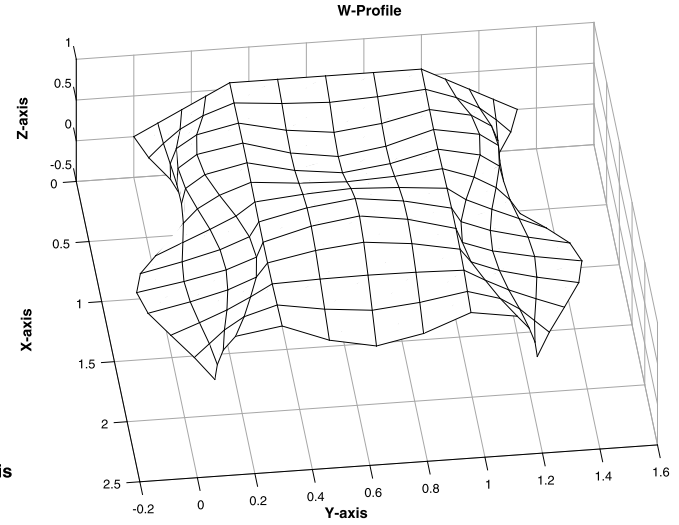

Mode 1, $\beta = 120^0$.

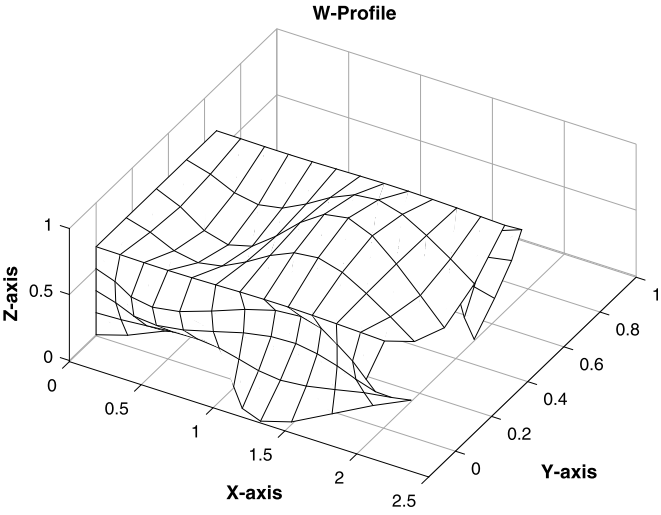

Mode 2, $\beta = 90^0$.

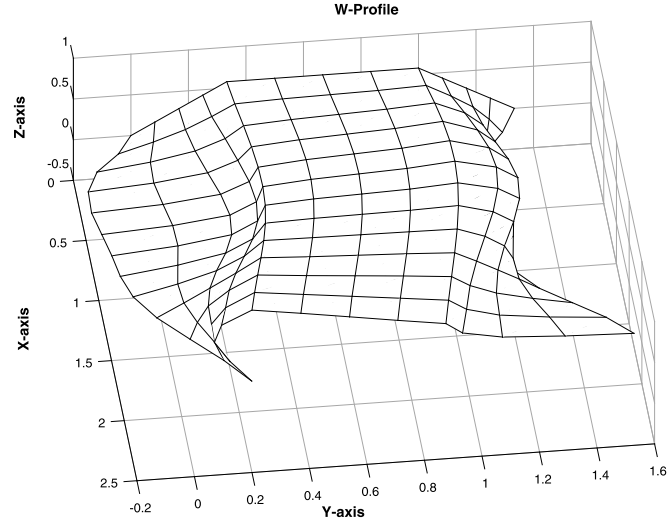

Mode 2, $\beta = 120^0$.

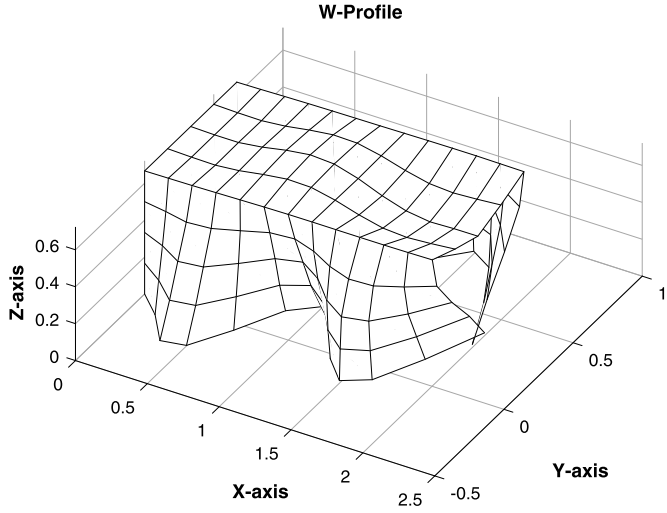

Mode 3, $\beta = 90^0$.

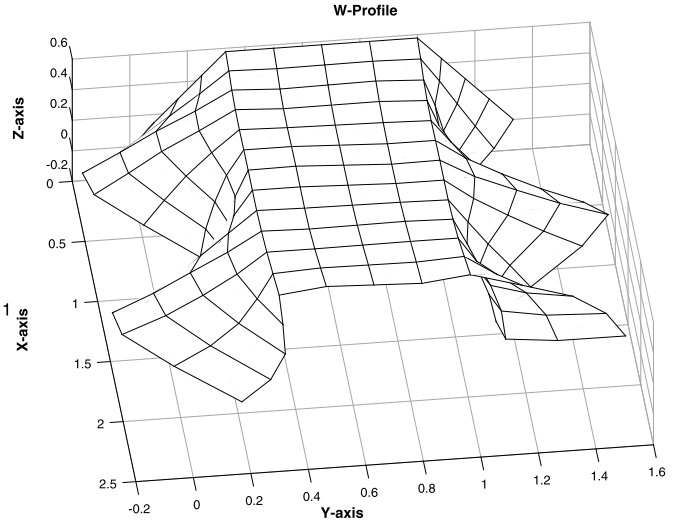

Mode 3, $\beta = 120^0$.

Fig. 4. First three mode shape of two-fold folded isotropic plate for crank angle 90^0 and 120^0.

Table 3
Nondimensional natural frequency ($\bar{\omega}$) of cantilever isotropic two-folded square plate.

Fold angle	Mode number	$\bar{\omega} = \omega a\sqrt{\rho(1-\nu^2)/E}$		
		Present	Niyogi et al. [28]	Liu et al. [8]
90^0	1	0.1231	0.1249	0.1249
	2	0.1245	0.1252	0.1260
	3	0.2553	0.2697	0.2579
	4	0.2677	0.2830	0.2892
	5	0.3190	0.3266	0.3286
120^0	1	0.0969	0.0971	0.100
	2	0.1237	0.1239	0.1241
	3	0.2545	0.2578	0.2571
	4	0.2611	0.2691	0.2630
	5	0.2897	0.2906	0.2986
150^0	1	0.0668	0.0679	0.0687
	2	0.1134	0.1142	0.1145
	3	0.2059	0.2065	0.2100
	4	0.2378	0.2410	0.2415
	5	0.2541	0.2573	0.2571

Table 4
Nondimensional natural frequency ($\bar{\omega}$) of two-fold folded isotropic plate under CFCF boundary condition.

Crank angle	a/h	$\bar{\omega} = \omega a\sqrt{\rho(1-\nu^2)/E}$				
		Mode 1	Mode 2	Mode 3	Mode 4	Mode 5
90^0	10	0.8249	0.9255	1.2520	1.5785	1.6140
	50	0.2088	0.2280	0.4432	0.4538	0.7134
	100	0.1050	0.1157	0.2235	0.2293	0.3719
120^0	10	0.7566	0.8973	1.1940	1.6528	1.7415
	50	0.2087	0.2230	0.4430	0.4517	0.7076
	100	0.1050	0.1150	0.2235	0.2291	0.3718
150^0	10	0.7050	0.7551	1.1242	1.6782	1.6867
	50	0.2040	0.2070	0.4407	0.4417	0.5992
	100	0.1048	0.1117	0.2232	0.2276	0.3649

Table 5
Nondimensional natural frequency ($\bar{\omega} = \omega a\sqrt{\rho(1-\nu^2)/E}$) of isotropic two-fold folded plate under SFCF boundary condition ($X = 0$ simply supported, $X = a$ clamped, $Y = 0$ and $Y = b$ are free).

Crank angle	Source	Mode					
		1	2	3	4	5	6
90^0	Present	0.2382	0.2943	0.4512	0.4817	0.5243	0.6332
	Haldar and Sheikh [31]	0.2365	0.2912	0.4489	0.4782	0.5180	0.630
	Liu and Huang [8]	0.2350	0.2900	0.4450			
120^0	Present	0.2219	0.2660	0.4258	0.4404	0.4743	0.6127
	Haldar and Sheikh [31]	0.2187	0.2617	0.4237	0.4340	0.4649	0.609
	Liu and Huang [8]	0.2200	0.2600	0.4250			
150^0	Present	0.2202	0.2220	0.3289	0.4381	0.4532	0.5338
	Haldar and Sheikh [31]	0.2174	0.2195	0.3283	0.4323	0.4461	0.529
	Liu and Huang [8]	0.2150	0.2175	0.3250			

3.3.4. Free vibration of two-fold folded laminated composite plate

In this section, the two-fold folded laminated composite plates are analyzed for various fold angle, lamination schemes, and boundary conditions. The material properties used for the composite plate are MM2 with side-to-thickness ratio, $a/h = 50$. The two-fold cantilever (CFFF, one of the folded side clamped) plate with $a = b = 2$ m is considered for the evaluation of nondimensional natural frequencies. The obtained solutions for the same are shown in Table 9. Unlike one-fold laminated composite plate, the two-fold folded laminated composite plate gives significantly different natural frequency for different crank angle and the frequencies are found to be decreasing with increase in fold angle. The present solutions are compared with the available solution from the literature and found to be in well agreement.

Further, the two fold laminated composite plate with various fold angle and lamination scheme under clamped-clamped (CFCF, both folded side clamped) boundary condition is also analyzed and the obtained solutions are presented in Table 10. It is observed that in this case also the natural frequency decreases with increase in crank angle due to decrease of in-plane stiffness contribution in flexural rigidity. Moreover, this problem is also analyzed for SFCF and SSSS boundary condition, and the obtained solutions are presented in Table 11. It is observed that the nondimensional natural frequency of SSSS boundary condition is more than the SFCF boundary condition due to more number of overall constraints in the SSSS boundary condition.

In addition, the same problem is also analyzed by ANSYS software for CFFF and CFCF boundary condition and the obtained solutions are presented in Table 12. The ANSYS results are in well agreement with the MATLAB FEM code computed solution as mentioned in Tables 9 and 10. The ANSYS solutions show some discrepancies due to FSDT being employed in the software.

Table 6
Nondimensional natural frequencies ($\bar{\omega}$) for one-fold folded laminated composite cantilever (CFFF) plate.

Crank angle	Ply-orientation	$\bar{\omega} = \omega a\sqrt{\rho(1-\nu_{12}^2)/E_1}$					
		Niyogi et al. (FSDT) [28]			Present (IHSDT)		
		Mode 1	Mode 2	Mode 3	Mode 1	Mode 2	Mode 3
90^0	$[30^0/-30^0/30^0]$	0.0390	0.0712	0.1473	0.0416	0.0718	0.1489
	$[45^0/-45^0/45^0]$	0.0381	0.0753	0.1406	0.0412	0.0753	0.1451
	$[60^0/-60^0/60^0]$	0.0367	0.0804	0.1399	0.0386	0.0797	0.1367
120^0	$[30^0/-30^0/30^0]$	0.0390	0.0697	0.1472	0.0417	0.0704	0.1491
	$[45^0/-45^0/45^0]$	0.0381	0.0731	0.0768	0.0414	0.0731	0.1448
	$[60^0/-60^0/60^0]$	0.0366	0.0768	0.1331	0.0388	0.0764	0.1366
150^0	$[30^0/-30^0/30^0]$	0.0389	0.0624	0.1455	0.0417	0.0629	0.1477
	$[45^0/-45^0/45^0]$	0.0380	0.0629	0.1377	0.0413	0.0626	0.1409
	$[60^0/-60^0/60^0]$	0.0366	0.0624	0.1306	0.0387	0.0621	0.1327
180^0	$[30^0/-30^0/30^0]$	0.0177	0.0387	0.1015	0.0170	0.0412	0.1038
	$[45^0/-45^0/45^0]$	0.0158	0.0378	0.0948	0.0149	0.0411	0.0922
	$[60^0/-60^0/60^0]$	0.0141	0.0364	0.0862	0.0136	0.0388	0.0843

Table 7
Nondimensional natural frequency ($\bar{\omega}$) of one-fold folded laminated composite plate under CFCF boundary condition.

Crank angle	a/h	$\bar{\omega} = \omega a\sqrt{\rho(1-\nu_{12}^2)/E_1}$					
		$[45^0/-45^0/45^0]$			$[0^0/90^0/0^0]$		
		Mode 1	Mode 2	Mode 3	Mode 1	Mode 2	Mode 3
90^0	10	0.5340	0.6080	1.1727	0.6147	0.6700	1.0638
	50	0.1208	0.1399	0.2994	0.1400	0.1541	0.3204
	100	0.0608	0.0704	0.1511	0.0704	0.0774	0.1616
120^0	10	0.5354	0.5807	1.0595	0.6158	0.6515	0.9782
	50	0.1208	0.1395	0.2994	0.1400	0.1538	0.3211
	100	0.0608	0.0704	0.1511	0.0704	0.0774	0.1617
150^0	10	0.5133	0.5350	0.9331	0.6081	0.6162	0.8884
	50	0.1207	0.1375	0.2983	0.1400	0.1526	0.3213
	100	0.0608	0.0701	0.1510	0.0704	0.0773	0.1618

Table 8
Nondimensional natural ($\bar{\omega}$) frequency of one-fold folded composite plate having $a/h = 50$ by ANSYS software.

Crank angle	Ply-orientation	$\bar{\omega} = \omega a\sqrt{\rho(1-\nu_{12}^2)/E_1}$					
		CFFF			CFCF		
		Mode 1	Mode 2	Mode 3	Mode 1	Mode 2	Mode 3
90^0	$[30^0/-30^0/30^0]$	0.0418	0.0719	0.1550	0.1369	0.1515	0.3660
	$[45^0/-45^0/45^0]$	0.0413	0.0754	0.1510	0.1267	0.1448	0.3626
	$[60^0/-60^0/60^0]$	0.0388	0.0796	0.1431	0.1168	0.1404	0.3341
120^0	$[30^0/-30^0/30^0]$	0.0418	0.0702	0.1549	0.1369	0.1512	0.3667
	$[45^0/-45^0/45^0]$	0.0414	0.0728	0.1508	0.1267	0.1445	0.3627
	$[60^0/-60^0/60^0]$	0.0388	0.0759	0.1426	0.1168	0.1399	0.3341
150^0	$[30^0/-30^0/30^0]$	0.0404	0.0638	0.1431	0.1368	0.1498	0.3670
	$[45^0/-45^0/45^0]$	0.0412	0.0638	0.1483	0.1265	0.1426	0.3619
	$[60^0/-60^0/60^0]$	0.0404	0.0638	0.1431	0.1167	0.1376	0.3335
180^0	$[30^0/-30^0/30^0]$	0.0169	0.0412	0.1082	0.1194	0.1357	0.2052
	$[45^0/-45^0/45^0]$	0.0149	0.0410	0.0975	0.1047	0.1255	0.2066
	$[60^0/-60^0/60^0]$	0.135	0.0388	0.0892	0.0942	0.1163	0.2051

3.3.5. Effect of fold location on the natural frequencies of folded laminated composite plate

So far, the free vibration of folded plate is analyzed considering the fold location in the middle of the one side ($y = b/2$). However, in the practical case the fold can be anywhere in the plate as shown in Fig. 5a. So, considering these aspects of the real world problem like winglet design, etc., in this section, the variation of non-dimensional natural frequencies is plotted against the location of fold ($0.1b$, $0.2b$, $0.3b$..., b) along y-axis as shown in Fig. 5. The plate dimensions $a = b = 2$ m with material properties MM2 have been considered for the analysis. The variation of non-dimensional natural frequencies of one-fold folded laminated composite plate under CFFF

Table 9
Nondimensional natural frequencies ($\bar{\omega}$) for two-folded laminated composite cantilever plate.

Folding angle	Ply-orientation	$\bar{\omega} = \omega a\sqrt{\rho(1-\nu_{12}^2)/E_1}$					
		Lee et al. (HSDT) [29]			Present (IHSDT)		
		Mode 1	Mode 2	Mode 3	Mode 1	Mode 2	Mode 3
90^0	$[30^0/-30^0]_s$	0.0925	0.1128	0.2057	0.0916	0.0988	0.2103
	$[0^0/90^0]_s$	0.1055	0.1156	0.1990	0.0902	0.0946	0.2029
	$[0^0/90^0]_2$	0.0982	0.1068	0.2008	0.0999	0.1006	0.1977
	$[45^0/-45^0/45^0]$	0.0897	0.1102	0.2068	0.0915	0.1033	0.2079
120^0	$[30^0/-30^0]_s$	0.0736	0.1096	0.2017	0.0725	0.1061	0.2022
	$[0^0/90^0]_s$	0.0821	0.1132	0.1976	0.0804	0.1108	0.1958
	$[0^0/90^0]_2$	0.0807	0.1027	0.1992	0.0792	0.0998	0.1982
	$[45^0/-45^0/45^0]$	0.0758	0.1038	0.2040	0.0755	0.0995	0.2057
150^0	$[30^0/-30^0]_s$	0.0522	0.0948	0.1595	0.0513	0.0918	0.1561
	$[0^0/90^0]_s$	0.0537	0.1016	0.1760	0.0522	0.0993	0.1749
	$[0^0/90^0]_2$	0.0518	0.0923	0.1634	0.0531	0.0921	0.1704
	$[45^0/-45^0/45^0]$	0.0550	0.0929	0.1649	0.0543	0.0897	0.1609

Table 10
Nondimensional natural frequency ($\bar{\omega}$) of two-fold folded laminated composite plate under CFCF boundary condition.

Folding angle	Ply-orientation	$\bar{\omega} = \omega a\sqrt{\rho(1-\nu_{12}^2)/E_1}$		
		Mode 1	Mode 2	Mode 3
90^0	$[30^0/-30^0]_s$	0.1721	0.1833	0.3765
	$[0^0/90^0]_s$	0.1713	0.1835	0.3915
	$[0^0/90^0]_2$	0.1653	0.1824	0.3538
	$[45^0/-45^0/45^0]$	0.1689	0.1813	0.3514
120^0	$[30^0/-30^0]_s$	0.1719	0.1809	0.3760
	$[0^0/90^0]_s$	0.1712	0.1808	0.3914
	$[0^0/90^0]_2$	0.1653	0.1784	0.3539
	$[45^0/-45^0/45^0]$	0.1687	0.1780	0.3507
150^0	$[30^0/-30^0]_s$	0.1704	0.1705	0.3726
	$[0^0/90^0]_s$	0.1703	0.1703	0.3905
	$[0^0/90^0]_2$	0.1628	0.1644	0.3529
	$[45^0/-45^0/45^0]$	0.1645	0.1668	0.3462

Table 11
Nondimensional natural frequency ($\bar{\omega} = \omega a\sqrt{\rho(1-\nu_{12}^2)/E_1}$) of two-fold folded laminated composite plate for SFCF and SSSS boundary condition.

Crank angle	Ply-orientation	SFCF			SSSS		
		Mode 1	Mode 2	Mode 3	Mode 1	Mode 2	Mode 3
90^0	$[30^0/-30^0/30^0]$	0.1653	0.1795	0.3287	0.7522	0.8738	1.0357
	$[45^0/-45^0/45^0]$	0.1682	0.1798	0.3487	0.6820	0.8172	1.0075
	$[60^0/-60^0/60^0]$	0.1703	0.1809	0.3703	0.6234	0.7636	0.9739
120^0	$[30^0/-30^0/30^0]$	0.1506	0.1588	0.2930	0.4580	0.4677	0.5927
	$[45^0/-45^0/45^0]$	0.1495	0.1598	0.3052	0.4258	0.4628	0.5765
	$[60^0/-60^0/60^0]$	0.1463	0.1587	0.3181	0.3919	0.4427	0.5526
150^0	$[30^0/-30^0/30^0]$	0.1325	0.1483	0.2867	0.3234	0.4736	0.5314
	$[45^0/-45^0/45^0]$	0.1374	0.1495	0.2985	0.3247	0.4376	0.5249
	$[60^0/-60^0/60^0]$	0.1386	0.1492	0.3122	0.3229	0.4005	0.4955

(one of the folded side clamped) boundary condition for various crank angle is shown in Fig. 5b. It can be observed that the variation in nondimensional natural frequencies is symmetric about the middle ($y = b/2$) axis for the three-layered cross-ply $[0^0/90^0/0^0]$ laminated plate, whereas the same is not true for the three-layered angle-play $[45^0/-45^0/45^0]$ laminated composite plate due to the combined effect of fiber-orientation and boundary condition. Also, the maximum value of first natural frequencies is found at the middle fold location because the maximum extensional stiffness of the plate is found there. This observation vindicates the optimum design found in nature like Palm leaves, etc.

Table 12
Nondimensional natural frequency ($\bar{\omega}$) of two-fold folded laminated composite plate by ANSYS.

Crank angle	Ply-orientation	$\bar{\omega} = \omega a\sqrt{\rho(1-\nu_{12}^2)/E_1}$					
		CFFF			CFCF		
		Mode 1	Mode 2	Mode 3	Mode 1	Mode 2	Mode 3
90^0	$[30^0/-30^0]_s$	0.0922	0.1079	0.2117	0.1721	0.1885	0.3547
	$[0^0/90^0]_s$	0.0989	0.1083	0.2038	0.1703	0.1904	0.3453
	$[0^0/90^0]_2$	0.0989	0.0999	0.2017	0.1667	0.1839	0.3756
	$[45^0/-45^0/45^0]$	0.0898	0.1025	0.2099	0.1695	0.1829	0.3710
120^0	$[30^0/-30^0]_s$	0.0718	0.995	0.2066	0.1710	0.1850	0.3536
	$[0^0/90^0]_s$	0.0771	0.1058	0.2020	0.1693	0.1865	0.3444
	$[0^0/90^0]_2$	0.0769	0.0993	0.2011	0.1666	0.1800	0.3755
	$[45^0/-45^0/45^0]$	0.0715	0.0931	0.2058	0.1685	0.1798	0.3689
150^0	$[30^0/-30^0]_s$	0.501	0.0901	0.1551	0.1600	0.1656	0.3475
	$[0^0/90^0]_s$	0.0509	0.0975	0.1736	0.1577	0.1623	0.3377
	$[0^0/90^0]_2$	0.0518	0.0907	0.1689	0.1636	0.1651	0.3739
	$[45^0/-45^0/45^0]$	0.0529	0.0884	0.1596	0.1653	0.1674	0.3656

Now, the same variation is studied for the FCFF (one of the unfolded side clamped) boundary condition and the obtained non-dimensional natural frequencies are plotted against the fold location as shown in Fig. 5c. It can be observed that unlike one of the folded side clamped condition, in this case, the results are symmetric about the middle ($y = b/2$) axis for both cross-ply $[0^0/90^0/0^0]$ and angle-ply $[45^0/-45^0/45^0]$ laminated composite plate. Moreover, the non-dimensional frequencies are much smaller than the previous counterpart shown in Fig. 5b. Further, the variation of non-dimensional natural frequencies for different fold location is studied for CFCF (both folded side clamped) boundary condition and the results are presented in Fig. 5d. The same solution for FCFC (both unfolded side clamped) boundary condition is shown in Fig. 5e. It is observed that both the results show the symmetry about middle ($y = b/2$) axis due to symmetry in the boundary condition.

In a nutshell, it can be said that the folded plate frequencies are highly affected by the boundary conditions and lamination scheme of the laminated composite plate as well as the fold location. This variation study of the non-dimensional natural frequencies against the fold location may be utilized for proper utilization of real folded plate structure.

3.4. Transient analysis

In this subsection, the transient analysis of folded laminated composite plate is discussed with standard problems. The one-fold and two-fold folded laminated composite plates are considered under the uniform pressure step loading and vertical loading. The Newmark's time integration scheme has been employed to solve the temporal partial governing differential equations of motion. The Newmark's coefficients used in the analysis are $\alpha = 0.5$ and $\beta = 0.25$. The time step for the Newmark approach has been selected by the method given by Tsui and Tong [48]. The solution has been obtained for various boundary conditions.

3.4.1. Transient analysis of one-fold folded laminated composite plate

A two-layered one-fold folded laminated $[30^0/-30^0]$ composite cantilever plate is considered for the transient analysis. The plate is made of material properties MM2 and has dimension as $a = b = 1.5$ m with $a/h = 50$. A pressure step load with intensity 1×10^5 N/m^2 is applied for $t_1 = 0.01$ s to get the forced response of the plate. The response of the central tip ($X = a, Y = b/2$; considering flat plate) deflection for the fold angle 120^0 and 90^0 are obtained using time-step $\Delta t = 5 \times 10^{-6}$ s and the solutions are shown in Fig. 6a. The obtained response is compared and validated with the available solution of Niyogi et al. [28] and the response is found to be in well agreement. The solution is also validated by ANSYS software solution as shown in Fig. 6a. A little difference is observed in the response due to utilization of FSDT in the ANSYS software solution. It is observed in Fig. 6a that the transient deflection for 120^0 crank angle is more than the 90^0 crank angle due to decrease in rigidity with increase in fold angle. Further, the difference between the deflection for 120^0 and 90^0 crank angle increases with time.

Further, the same problem is considered under the clamped-clamped (CFCF) boundary condition and the central tip (point B, Fig. 2a) deflection is obtained for crank angle, $\beta = 90^0$, 120^0, and 150^0 which are shown in Fig. 6b. The solution is again compared with the ANSYS software solution and found to be in good agreement. It can be observed from Fig. 6b that the magnitude of central tip deflection increases with increase in the crank angle of folded plate. Moreover, in the case of CFCF boundary condition, the difference in deflection for various crank angle is not as contrast as in the CFFF due to both folded side constraint.

3.4.2. Transient analysis of two-fold folded laminated composite plate

In this part, a two-layered double folded laminated composite plate with different lamination schemes, fold angle, and boundary conditions have been considered for the transient analysis. The plate having dimensions $a = b = 1.5$ m with $a/h = 50$ is made of material properties MM2. A transverse step load with intensity 1×10^5 N/m^2 is applied for the $t_1 = 0.01$ s and obtained responses are shown in Fig. 7. The central tip (point B', Fig. 2b) deflection of cantilever laminated composite plate is obtained for two different fiber-orientation for crank angle 120^0 and the obtained solutions are shown in Fig. 7a. The solution is also compared with the results obtained from ANSYS software and found to be in good agreement as shown in Fig. 7a. It is observed from the Fig. 7a that the transverse central tip (point B') deflection for the lamination scheme $[60^0/-60^0]$ is found to be more than the $[30^0/-30^0]$ due to decrease in flexural stiffness with increase in the fiber-orientation angle. Further, Fig. 7b shows the central tip (point B') deflection of two-fold folded laminated $[30^0/-30^0]$

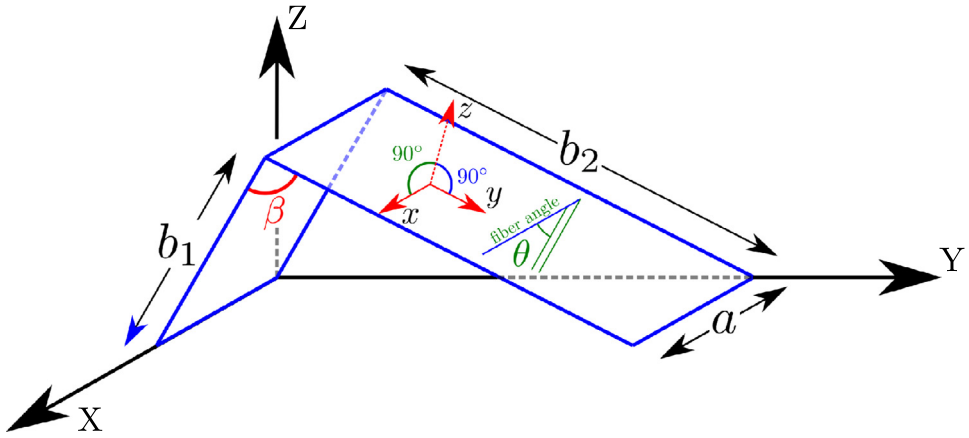

(a) Schematic diagram for one-fold folded plate with varying b_1 and b_2.

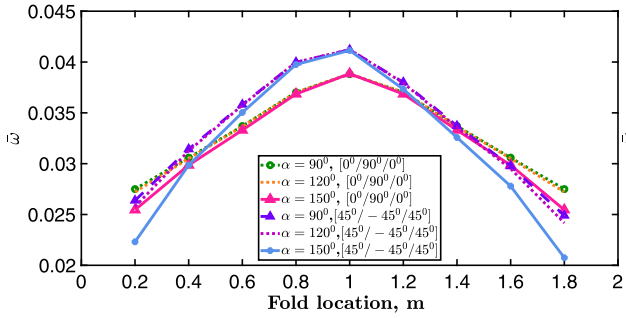

(b) CFFF (one of the folded side clamped).

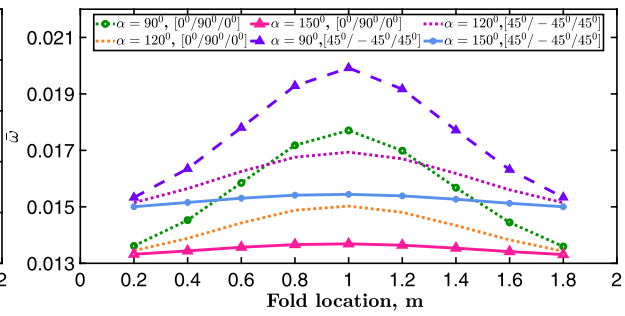

(c) FCFF (one unfolded side clamped).

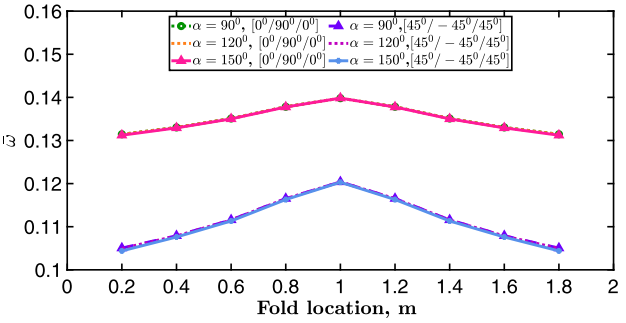

(d) CFCF (two folded side clamped).

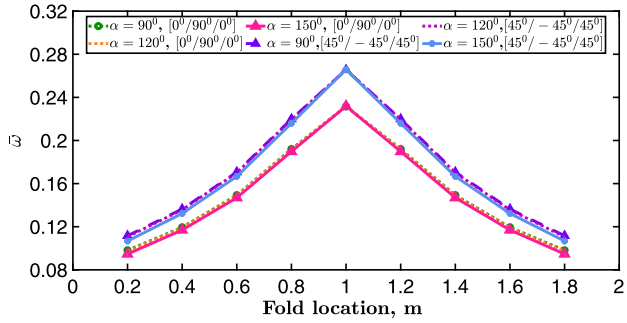

(e) FCFC (two unfolded side clamped).

Fig. 5. Variation of nondimensional natural frequencies for different fold location of one-fold folded laminated composite plate under various boundary condition and crank angle. (For interpretation of the colors in the figure(s), the reader is referred to the web version of this article.)

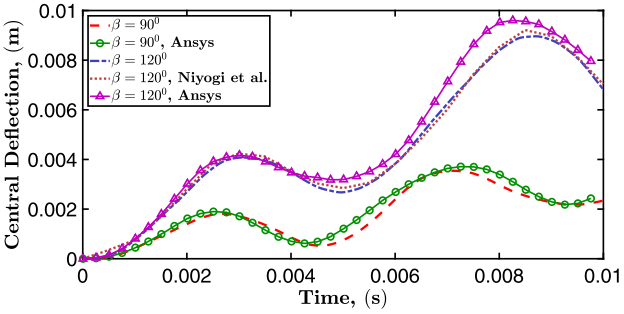

(a) Transverse tip deflection of single folded laminated $[30^0/-30^0]$ composite cantilever plate subjected to uniformly distributed step loading with intensity $1 \times 10^5\ N/m^2$ for crank angle $\beta = 120^0$.

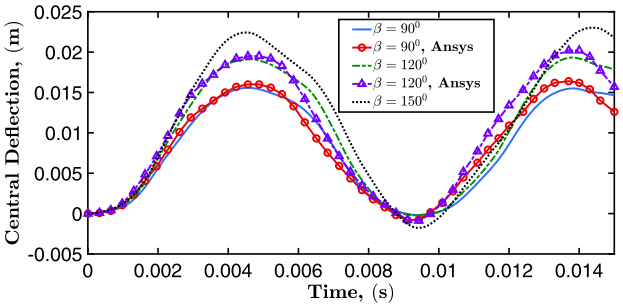

(b) Central tip deflection of one-fold folded laminated composite $[30^0/-30]$ plate under CFCF boundary condition for load intensity $1 \times 10^5 N/m^2$.

Fig. 6. Transient deflection response one-fold folded laminated composite plate for various boundary condition and crank angle.

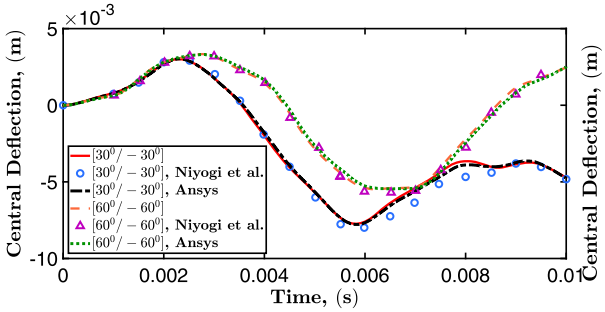

(a) Transverse deflection of tip (point B') of a two-fold folded laminated composite plate with fold angle 120^0 under CFFF(one of the folded side clamped) boundary condition.

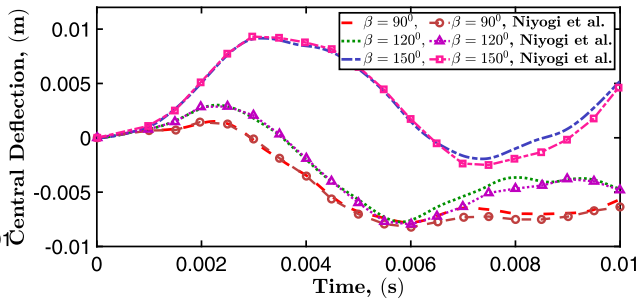

(b) Central tip (point B') deflection of two-fold folded laminated composite $[30^0/-30]$ plate under CFFF (one of the folded side clamped) boundary condition.

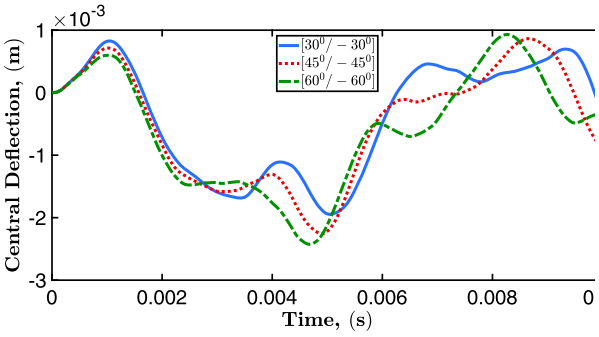

(c) Central (point A') deflection of two-fold folded laminated composite plate for crank angle 120^0 under CFCF (both folded side clamped) boundary condition.

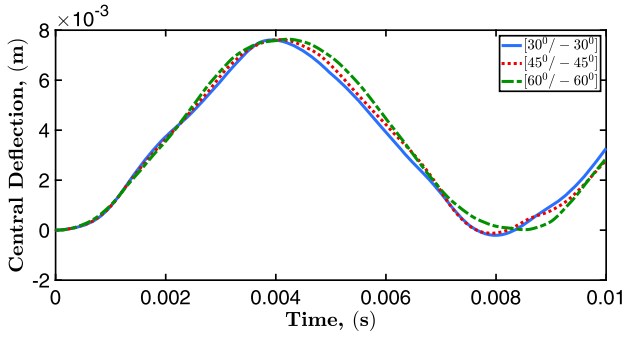

(d) Central tip (point B') deflection of two-fold folded laminated composite plate for crank angle 120^0 under CFCF boundary condition.

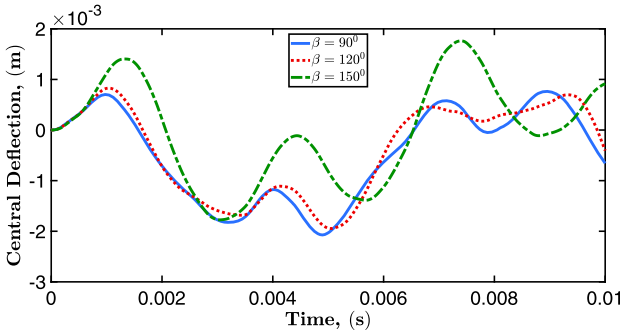

(e) Central (point A') deflection of two-fold folded laminated $[30^0/-30^0]$ composite plate under CFCF boundary condition for various crank angle.

Fig. 7. Transient deflection response of two-fold folded laminated composite plate under uniform pressure load of intensity 1×10^5 N/m^2.

composite cantilever (CFFF) plate for crank angle $\beta = 90^0, 120^0$ and 150^0. The obtained responses are compared with the available solution of Niyogi et al. [28] and the responses are found to be in good agreement. It is observed that the central tip (point B') deflection increases with increase in crank angle due to decrease in the flexural rigidity.

Further, the same problem is considered for the clamped-clamped (CFCF, both folded side clamped) boundary condition and the obtained central (point A') deflection is shown in Fig. 7c. Moreover, the central tip (point C') deflection response has also been obtained and shown in Fig. 7d. Further, the response for varying crank angle under clamped-clamped (CFCF) boundary condition is also obtained and shown in Fig. 7e. Unlike cantilever two-fold folded plate, the folded plate under CFCF boundary conditions shows no pattern of variation with respect to fiber-orientation due to complex effect of crank angle and boundary constraints. Same thing is observed with the crank angle variation as shown in Fig. 7e.

3.4.3. Transient analysis of folded laminated composite plate under vertical load

So far, the transient solution is obtained for the applied pressure load, however, the most prominent type of loading in the actual folded structure is the vertical load (parallel to global Z-axis) which is inclined to the local plane at some angle other than the 90^0. Hence, in this section, the problems are analyzed under the applied vertical load as shown in Figs. 8a and 9a, and the transient displacement solutions are obtained at different location for various boundary conditions. The plate dimensions $a = b = 1.5$ m and $a/h = 50$ with material properties MM2 are considered for the analysis. The vertical load of magnitude 10^5 N/m^2 is applied for $t_1 = 0.01$ s. The transient displacement response using time-step $\Delta t = 1 \times 10^5$ s is obtained.

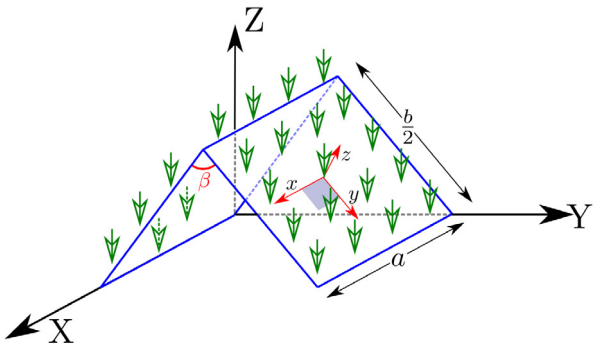

(a) Schematic diagram of one-fold folded plate under vertical load parallel to global Z-axis.

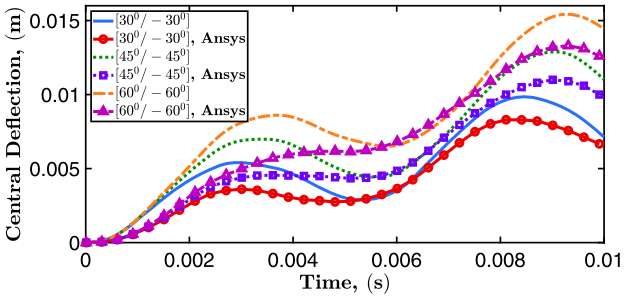

(b) Central tip (point B) deflection of one-fold folded laminated composite plate under vertical applied load and CFFF (one folded side clamped) boundary condition for crank angle 120^0.

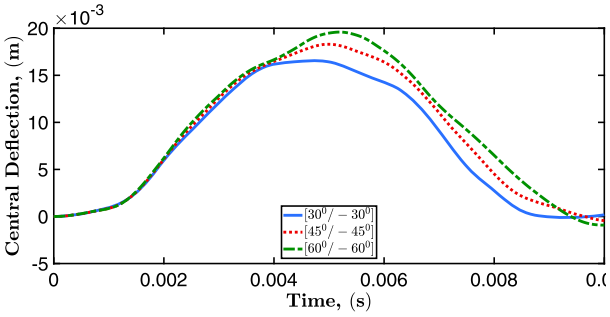

(c) Central tip (point C) deflection of one-fold folded laminated composite plate under vertical applied load and CFCF (both folded side clamped) boundary condition for crank angle 120^0.

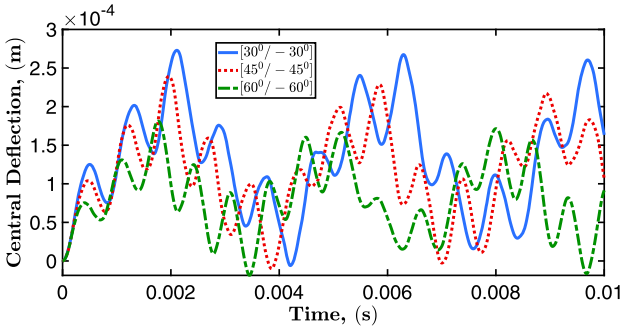

(d) Central tip (point B) deflection of one-fold folded laminated composite plate under vertical applied load and FCFC (both unfolded side clamped) boundary condition.

Fig. 8. Transient deflection response of one-fold folded laminated composite plate under vertical load.

The central tip (point B) deflections of one-fold folded laminated composite plate under vertical applied load and CFFF (one of the folded side clamped) boundary condition for crank angle 120^0 and various lamination schemes are shown in Fig. 8b. This solution has also been compared with the ANSYS solution and found to be at large discrepancy than the uniform pressure load solution due to negligence of one component of the vertical load in the ANSYS. As ANSYS only allows directional load to be applied at the node while in the present case it has been applied at whole area. Like the pressure load, in this case also, the deflection is increasing with time for the cantilever boundary condition. Further, the central tip deflections are obtained for CFCF (both folded side clamped) boundary condition under applied vertical load of magnitude 10^5 N/m^2 and the solutions are shown in Fig. 8c. Also, the central tip (point B) deflections of one-fold folded laminated composite plate under FCFC (both unfolded side clamped) boundary condition are obtained and the solutions are shown in Fig. 8d. It is observed that in case of CFCF boundary condition, the central tip (point C) deflection increases with increase in fiber-angle. Whereas, for the FCFC boundary condition, the central tip (point B) of one-fold folded laminated composite plate increases with decrease in fiber-orientation.

In addition, the central tip (point C') deflection of two-fold folded laminated composite plate under vertical load for CFCF (both folded side clamped) boundary condition has also been obtained and shown in Fig. 9b. An ANSYS solution has also been compared with this solution as shown in Fig. 9b. Again, the ANSYS solution shows large differences for the vertical load to the two-fold folded plate as it neglect the one component of applied load. Also, the ANSYS solution gives more deflection than the MATLAB-FEM code computed solution due to utilization of FSDT in the ANSYS. Further, the central tip (point B') deflection of two-fold folded laminated composite plate under FCFC (both unfolded side clamped) boundary condition has been obtained and shown in Fig. 9c. Like the one-fold folded plate, the central (point A') deflection of two-fold folded plate under vertical load increases with decrease in fiber-orientation for the FCFC boundary condition.

4. Conclusion

The one-fold and two-fold folded laminated composite plate are analyzed using efficient nine noded C^0 continuity FEM-IHSDT model for the free and forced vibration. In the first part, the non-dimensional natural frequencies are obtained for the various lamination schemes, fold angles, and boundary conditions. Moreover, considering the real world problem like winglet design, etc., the non-dimensional natural frequencies for different fold locations are also obtained to assess the free vibration behavior of folded structure. In the second part, the transient analyses are carried out for the cantilever and clamped-clamped laminated composite plate under the consideration of one-fold and two-fold structure. For the forced vibration analysis, a pressure load as well as a vertical load parallel to global Z-axis has been employed. The central-tip and central deflection are obtained for the various boundary conditions, lamination schemes, and crank angles. The obtained solutions are extensively validated with the available results from the literature and the obtained ANSYS software solution; and are found to be performing well. These validations show the effectiveness of the inverse hyperbolic shear deformation theory (IHSDT) for the dynamic analysis of folded laminated composites plate. It is observed that the first non-dimensional natural frequency of one-fold isotropic plate is found to be almost same for different crank angle; and are significantly different than the flat plate. The same is

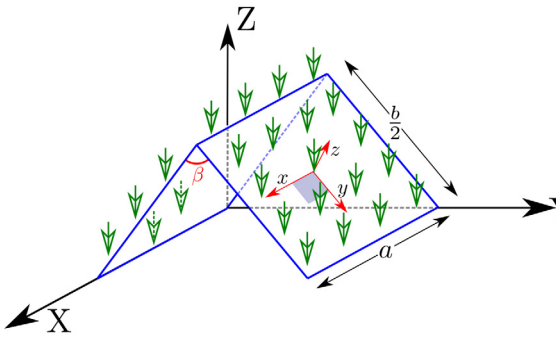

(a) Schematic diagram of two-fold folded plate under vertical load parallel to global Z-axis.

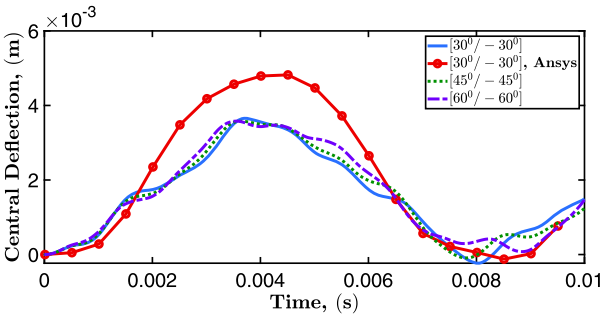

(b) Central tip (point C') deflection of two-fold folded laminated composite plate under applied vertical load and CFCF (both folded side clamped) boundary condition.

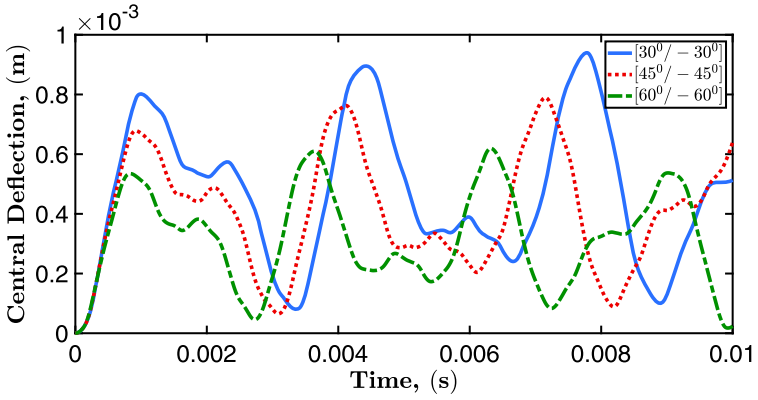

(c) Central (point A') deflection of two-fold folded laminated composite plate under applied vertical load and FCFC (both unfolded side clamped) boundary condition.

Fig. 9. Transient deflection response of two-fold folded laminated composite plate under vertical load.

observed for the one-fold laminated composite plate. However, in the case of two-fold laminated composite plate, the non-dimensional natural frequencies are found to be significantly different for different fold angles. Further, the analysis suggests that the stiffness of two-fold folded laminated composite plate is more susceptible to crank angle than the one-fold folded plate. Moreover, the present analysis also vindicates the optimized design of the natural folded structure like Palm leaves, etc., which possess a symmetry in its folding pattern.

Declaration of competing interest

The authors declare that they have no known competing financial interests or personal relationships that could have appeared to influence the work reported in this paper.

References

[1] J. Goldberg, H. Leve, Theory of prismatic folded plate structures, IABSE J. 17 (1957).
[2] T. Irie, G. Yamada, Y. Kobayashi, Free vibration of a cantilever folded plate, J. Acoust. Soc. Am. 76 (6) (1984) 1743–1748, https://doi.org/10.1121/1.391622.
[3] M. Ohga, T. Shigematsu, Bending analysis of plates with variable thickness by boundary element-transfer matrix method, Comput. Struct. 28 (5) (1988) 635–640, https://doi.org/10.1016/0045-7949(88)90008-9.
[4] B.W. Golley, W.A. Grice, Prismatic folded plate analysis using finite strip-elements, Comput. Methods Appl. Mech. Eng. 76 (2) (1989) 101–118, https://doi.org/10.1016/0045-7825(89)90090-X.
[5] A.L. Eterovic, L.A. Godoy, An exact strip method for folded plate structures, Comput. Struct. 32 (2) (1989) 263–276, https://doi.org/10.1016/0045-7949(89)90038-2.
[6] J. Bandyopadhyay, P. Laad, Comparative analysis of folded plate structures, Comput. Struct. 36 (2) (1990) 291–296, https://doi.org/10.1016/0045-7949(90)90128-O.
[7] M. Ohga, T. Shigematsu, S. Kohigashi, Analysis of folded plate structures by a combined boundary element-transfer matrix method, Comput. Struct. 41 (4) (1991) 739–744, https://doi.org/10.1016/0045-7949(91)90183-M.
[8] W. Liu, C. Huang, Vibration analysis of folded plates, J. Sound Vib. 157 (1) (1992) 123–137, https://doi.org/10.1016/0022-460X(92)90570-N.
[9] A.N. Danial, Inverse solutions on folded plate structures, Ph.D. thesis, Purdue University, 1994.
[10] A. Danial, J. Doyle, S. Rizzi, Dynamic analysis of folded plate structures, J. Vib. Acoust. 118 (4) (1996) 591–598, https://doi.org/10.1115/1.2888339.
[11] M. Duan, Y. Miyamoto, Effective hybrid/mixed finite elements for folded-plate structures, J. Eng. Mech. 128 (2) (2002) 202–208, https://doi.org/10.1061/(ASCE)0733-9399(2002)128:2(202).
[12] E. Hernández, L. Hervella-Nieto, Finite element approximation of free vibration of folded plates, Comput. Methods Appl. Mech. Eng. 198 (15–16) (2009) 1360–1367, https://doi.org/10.1016/j.cma.2008.12.002.
[13] L. Peng, Free vibration analysis of symmetrically laminated folded plate structures using an element-free Galerkin method, Math. Probl. Eng. 2015 (2015), https://doi.org/10.1155/2015/124296.
[14] C. Kim, C. Son, Rapid design approach for u-bend of a turbine serpentine cooling passage, Aerosp. Sci. Technol. 92 (2019) 417–428, https://doi.org/10.1016/j.ast.2019.05.019.
[15] J.N. Reddy, A simple higher-order theory for laminated composite plates, J. Appl. Mech. 51 (4) (1984) 745–752, https://doi.org/10.1115/1.3167719.
[16] T. Kant, J. Varaiya, C. Arora, Finite element transient analysis of composite and sandwich plates based on a refined theory and implicit time integration schemes, Comput. Struct. 36 (3) (1990) 401–420, https://doi.org/10.1016/0045-7949(90)90279-B.

[17] M.A. Bennaceur, Y. Xu, Application of the natural element method for the analysis of composite laminated plates, Aerosp. Sci. Technol. 87 (2019) 244–253, https://doi.org/10.1016/j.ast.2019.02.038.
[18] D. Hu, X. Yi, M. Jiang, G. Li, X. Cong, X. Liu, C. Rudd, Development of highly electrically conductive composites for aeronautical applications utilizing bi-functional composite interleaves, Aerosp. Sci. Technol. (2020) 105669, https://doi.org/10.1016/j.ast.2019.105669.
[19] M. Aydogdu, A new shear deformation theory for laminated composite plates, Compos. Struct. 89 (1) (2009) 94–101, https://doi.org/10.1016/j.compstruct.2008.07.008.
[20] M. Karama, K. Afaq, S. Mistou, A new theory for laminated composite plates, Proc. Inst. Mech. Eng. L, J. Mat. Des. Appl. 223 (2) (2009) 53–62, https://doi.org/10.1243/14644207JMDA189.
[21] N. El Meiche, A. Tounsi, N. Ziane, I. Mechab, et al., A new hyperbolic shear deformation theory for buckling and vibration of functionally graded sandwich plate, Int. J. Mech. Sci. 53 (4) (2011) 237–247, https://doi.org/10.1016/j.ijmecsci.2011.01.004.
[22] J. Mantari, A. Oktem, C.G. Soares, A new higher order shear deformation theory for sandwich and composite laminated plates, Composites, Part B, Eng. 43 (3) (2012) 1489–1499, https://doi.org/10.1016/j.compositesb.2011.07.017.
[23] J. Mantari, A. Oktem, C.G. Soares, A new trigonometric shear deformation theory for isotropic, laminated composite and sandwich plates, Int. J. Solids Struct. 49 (1) (2012) 43–53, https://doi.org/10.1016/j.ijsolstr.2011.09.008.
[24] N. Grover, B. Singh, D. Maiti, New nonpolynomial shear-deformation theories for structural behavior of laminated-composite and sandwich plates, AIAA J. 51 (8) (2013) 1861–1871, https://doi.org/10.2514/1.J052399.
[25] S. Sarangan, B. Singh, Evaluation of free vibration and bending analysis of laminated composite and sandwich plates using non-polynomial zigzag models: C0 finite element formulation, Aerosp. Sci. Technol. 68 (2017) 496–508, https://doi.org/10.1016/j.ast.2017.06.001.
[26] A. Gupta, A. Ghosh, Isogeometric static and dynamic analysis of laminated and sandwich composite plates using nonpolynomial shear deformation theory, Composites, Part B, Eng. 176 (2019) 107295, https://doi.org/10.1016/j.compositesb.2019.107295.
[27] R. Suresh, S. Malhotra, Vibration and damping analysis of thin-walled box beams, J. Sound Vib. 215 (2) (1998) 201–210, https://doi.org/10.1006/jsvi.1996.1545.
[28] A. Guha Niyogi, M. Laha, P. Sinha, Finite element vibration analysis of laminated composite folded plate structures, Shock Vib. 6 (5–6) (1999) 273–283, https://doi.org/10.1155/1999/354234.
[29] S.-Y. Lee, S.-C. Wooh, S.-S. Yhim, Dynamic behavior of folded composite plates analyzed by the third order plate theory, Int. J. Solids Struct. 41 (7) (2004) 1879–1892, https://doi.org/10.1016/j.ijsolstr.2003.11.026.
[30] S.-Y. Lee, S.-C. Wooh, Finite element vibration analysis of composite box structures using the high order plate theory, J. Sound Vib. 277 (4–5) (2004) 801–814, https://doi.org/10.1016/j.jsv.2003.09.024.
[31] S. Haldar, A.H. Sheikh, Free vibration analysis of isotropic and composite folded plates using a shear flexible element, Finite Elem. Anal. Des. 42 (3) (2005) 208–226, https://doi.org/10.1016/j.finel.2005.06.003.
[32] K.S. Chun, S.K. Kassegne, Low-velocity impact dynamic behavior of laminated composite nonprismatic folded plate structures, J. Eng. Mech. 131 (7) (2005) 678–688, https://doi.org/10.1061/(ASCE)0733-9399(2005)131:7(678).
[33] U. Topal, Ü. Uzman, Frequency optimization of laminated folded composite plates, Mater. Des. 30 (3) (2009) 494–501, https://doi.org/10.1016/j.matdes.2008.05.066.
[34] A. Nayak, R. Shenoi, J. Blake, A study of transient response of initially stressed composite sandwich folded plates, Composites, Part B, Eng. 44 (1) (2013) 67–75, https://doi.org/10.1016/j.compositesb.2012.07.043.
[35] L. Le-Anh, T. Nguyen-Thoi, V. Ho-Huu, H. Dang-Trung, T. Bui-Xuan, Static and frequency optimization of folded laminated composite plates using an adjusted differential evolution algorithm and a smoothed triangular plate element, Compos. Struct. 127 (2015) 382–394, https://doi.org/10.1016/j.compstruct.2015.02.069.
[36] N. Nguyen-Minh, T. Nguyen-Thoi, T. Bui-Xuan, T. Vo-Duy, Static and free vibration analyses of stiffened folded plates using a cell-based smoothed discrete shear gap method (cs-fem-dsg3), Appl. Math. Comput. 266 (2015) 212–234, https://doi.org/10.1016/j.amc.2015.05.042.
[37] X. Zhang, H. Zhang, W. Ren, Bending collapse of folded tubes, Int. J. Mech. Sci. 117 (2016) 67–78, https://doi.org/10.1016/j.ijmecsci.2016.07.016.
[38] T.X. Bui, H.T. Dang, Analysis of static and free vibration of the sandwich folded plate using the layerwise theory, Sci. Technol.Dev. J. Nat. Sci. 1 (T5) (2017) 214–221, https://doi.org/10.32508/stdjns.v1iT5.555.
[39] C. Wang, H.H. Khodaparast, M.I. Friswell, Conceptual study of a morphing winglet based on unsymmetrical stiffness, Aerosp. Sci. Technol. 58 (2016) 546–558, https://doi.org/10.1016/j.ast.2016.09.015.
[40] J. Cai, Z. Ren, Y. Ding, X. Deng, Y. Xu, J. Feng, Deployment simulation of foldable origami membrane structures, Aerosp. Sci. Technol. 67 (2017) 343–353, https://doi.org/10.1016/j.ast.2017.04.002.
[41] A. Varshney, A.H. Khan, M.Y. Yasin, Z.A. Khan, M. Asjad, On the optimal dynamic design of laminated composite folded plates: a multi-criteria decision analysis, Multidiscip. Model. Mater. Struct. (2019), https://doi.org/10.1108/MMMS-06-2019-0116.
[42] M. Esposito, M. Gherlone, Composite wing box deformed-shape reconstruction based on measured strains: optimization and comparison of existing approaches, Aerosp. Sci. Technol. 99 (2020) 105758, https://doi.org/10.1016/j.ast.2020.105758.
[43] N. Grover, B. Singh, D. Maiti, Analytical and finite element modeling of laminated composite and sandwich plates: an assessment of a new shear deformation theory for free vibration response, Int. J. Mech. Sci. 67 (2013) 89–99, https://doi.org/10.1016/j.ijmecsci.2012.12.010.
[44] K. Bathe, Finite Element Procedures in Engineering Analysis, Prentice-Hall, Englewood Cliffs, 1982.
[45] J. Reddy, Mechanics of Laminated Composite Plates and Shells, Conservative, 2004.
[46] M.A. Bhatti, Advanced Topics in Finite Element Analysis of Structures: With Mathematica and MATLAB Computations, John Wiley & Sons, Inc., 2006.
[47] H. Mohammadi, A. Setoodeh, Fsdt-based isogeometric analysis for free vibration behavior of functionally graded skew folded plates, Iran. J. Sci. Technol. Trans. Mech. Eng. (2019) 1–23, https://doi.org/10.1007/s40997-019-00320-0.
[48] T.Y. Tsui, P. Tong, Stability of transient solution of moderately thick plate by finite-difference method, AIAA J. 9 (10) (1971) 2062–2063, https://doi.org/10.2514/3.6463.